Master in Chemical Engineering

Numerical analysis of water distribution inside a power transformer winding

A Master's dissertation

of

Leonardo de Figueiredo Alves e Teixeira Rodrigues

Developed within the course of dissertation

held in

Efacec Energia, Máquinas e Equipamentos Eléctricos, S.A.

Supervisor at FEUP: **Dr. Soraia Ferreira Neves**

Supervisor at Efacec: **Eng. Márcio Alexandre Quintela**

Departamento de Engenharia Química

July of 2018

Acknowledgments

Em primeiro lugar quero agradecer à Efacec pela oportunidade. Foi por um acaso que de duas passaram a ser três dissertações e pude fazer parte de tudo isto. Obrigado pelas condições disponibilizadas, pelo bom ambiente na empresa e pela ajuda não só a nível de conhecimentos, assim como financeira. Um obrigado especial ao Hugo Campelo.

À minha orientadora da faculdade, Soraia Neves, um enorme obrigado por todas as ajudas que me deste durante estes meses. Obrigado por toda a disponibilidade que tiveste, mesmo em alturas fora do horário de trabalho, para me fazeres perceber como efetivamente se devem fazer as coisas. É graças à tua orientação que o trabalho evoluiu e foi realizado com sucesso. Espero que não te tenha dado tanto trabalho como o outro Leonardo, e desejo tudo de bom para os dois.

Um grande obrigado a toda a Equipa de Fluidos e Calor. À Erica Doutel, quero agradecer todo o conhecimento transmitido sobre o *Fluent*, toda a ajuda no início para que me pudesse integrar no tema dos transformadores, área que para engenheiros químicos é "uma caixa negra". Obrigado por toda a boa disposição nas pausas, assim como as boleias que me fizeram poupar bastante tempo em transportes. À Ana Barradas, agradeço a predisposição para me ensinares como se devem criar geometrias e malhas adequadas à resolução dos problemas, assim como toda a alegria transmitida. Ao Márcio Quintela, agradeço toda a orientação especialmente numa fase mais final do trabalho, assim como a procura de outros caminhos e alternativas aos obstáculos encontrados durante a realização deste. À Sandra Couto, agradeço a disponibilidade para esclarecer todas as dúvidas, por mais estranhas que inicialmente tenham parecido. À Raquel Camacho, um obrigado por todas as dicas e sugestões feitas durante a realização do trabalho, assim como a boa disposição e gargalhadas partilhadas. Por último, um obrigado à Acília Coelho por toda a sapiência transmitida que só a experiência de muitos anos no mundo do trabalho é que podem fornecer. Foi um enorme prazer fazer parte desta equipa.

Quero agradecer à Elisabete Ferreira que me acompanhou nesta jornada nos dias bons e maus. A tua companhia e todas as conversas ajudaram a que as horas passassem sem me dar conta de tal, assim como adicionou uma camada de diversão a este projeto.

Um grande obrigado aos Aleatoriedades por toda a companhia ao longo do meu percurso académico, um grupo de pessoas espetaculares com as quais adorei fazer esta caminhada. Agora que estamos na etapa final, votos de que não nos afastemos muito, independentemente de para onde as nossas vidas rumarem.

Quero também agradecer ao Luís Caseiro, ao Miguel Figueiredo e ao João Miguel Rocha que já me acompanham desde uma tenra idade. A todos os nossos encontros, temas discutidos e aventuras passadas ao longo de mais de uma década, um grande obrigado.

Ao meu grande amigo Filipe Carvalho, quero agradecer todos os momentos que partilhámos. É um privilégio fazer projetos contigo, e ver todo o processo criativo transformado em realidade. Apesar das áreas de estudo bastante distintas, o mundo da música uniu-nos e fez-me conhecer uma pessoa fantástica.

Por último, quero agradecer à minha família. Aos meus pais, por serem dois pilares fundamentais na minha vida, e por me facultarem tudo o que sempre necessitei, dentro do possível. Ao meu irmão, por fazer com que a criança dentro de mim não desapareça.

Abstract

Nowadays more than ever the industry needs to understand the phenomena that occur inside a power transformer (PT). Several parameters are responsible for the degradation of the main insulators of a transformer (e.g. oil and paper), however the two most important ones are the temperature and water content. Water presence accelerates the ageing of the paper, which can cause partial discharges that, consequently, causes gas bubbles. These compromise the PT operation. For that reason, the main goal of this work was to study the water distribution inside the power transformer, specifically in the winding region, where a significant amount of paper can be exposed to water and high temperatures.

Computational Fluid Dynamics (CFD) simulations in steady-state were performed considering a 2D asymmetrical model of a disc-type winding. This study allowed to identify the locations inside the winding that will have the higher water concentration and where problems associated with water content may occur more intensely.

A first analysis on a winding pass was done and the flow and temperature distribution inside the geometry was obtained. Using the temperature distribution profile and the Oommen's equilibrium curves, the water content in the paper (WCP) on the discs surfaces was obtained for different water content in oil (WCO). Different methods were studied to estimate the paper water content (i.e. through the hot spot temperature, average temperature of the disc surface, average temperature of each disc surface and temperature distribution of the paper wrapped on discs). A second analysis was carried out on a winding. Different boundary conditions were considered and their effect on the temperature and WCP profiles of the winding were studied. The analysis of the temperature and WCP profiles obtained for three different values of WCO was done as well as the WCP calculation using different values of temperature. The WCP values on the most critical zones (disc surfaces where the WCP is higher) were determined and the deviation to average values is shown.

The results demonstrated the heterogeneous distribution of WCP along the winding discs where the higher values of WCP were obtained in the external regions of the discs. The aforementioned tendency increases with the augment of WCO. A significant difference between the WCP predictions of the hotter and cooler discs was obtained. The results also showed that predictions of water content in paper considering the hot spot temperature may be misleading since the estimated values can be less than half of the maximum value determined on critical conditions.

Keywords: Power transformers, winding, CFD, water content in paper, water content in oil, water distribution, heat transfer

Sumário

Hoje em dia a indústria necessita de compreender cada vez mais os fenómenos que decorrem dentro de um transformador de potência (PT). Existem vários parâmetros responsáveis pela degradação dos isolantes principais de um transformador (por exemplo óleo e papel), sendo os dois mais importantes a temperatura e o teor de água. A presença de água acelera o envelhecimento do papel, que pode causar descargas parciais que consequentemente levam à formação de gás. Isto compromete a operação de um PT. Por essa razão, o principal objetivo deste trabalho foi estudar a distribuição de água dentro de um transformador de potência, especificamente na região do enrolamento, onde uma quantidade significativa de papel pode estar exposta a água e a elevadas temperaturas.

Foram realizadas simulações CFD em estado estacionário considerando um modelo 2D axissimétrico de um enrolamento de um PT do tipo Core. Este estudo permite identificar a localização dentro do enrolamento que terá uma maior concentração de água e onde provavelmente os problemas associados com teor de água poderão ocorrer mais intensamente.

Uma primeira análise foi feita onde as distribuições de caudal e temperatura foram obtidas num passe do enrolamento. O teor de água no papel (WCP) nas superfícies dos discos foi calculado com base no perfil de distribuição de temperatura e nas curvas de equilíbrio de Oommen, para diferentes valores de teor de água no óleo (WCO). Foram estudados diferentes métodos para estimar o WCP (isto é, através da temperatura do ponto quente, temperatura média da superfície do disco, temperatura média de cada parede do disco e a distribuição de temperatura no papel enrolado nos discos). Foi também feita uma segunda análise considerando toda a geometria do enrolamento. Foram testadas diferentes condições de operação e os seus efeitos nos perfis de temperatura e WCO do enrolamento foram estudados. Foi feita uma análise aos perfis de temperatura obtidos para três valores de WCO assim como o cálculo do WCP usando diferentes valores de temperatura. Os valores de WCP nas zonas mais críticas (superfícies do disco onde o valor de WCP é maior) foram calculados assim como o desvio entre estes valores e os valores médios.

Os resultados demonstram a distribuição heterogénea de WCP dentro da superfície dos discos do enrolamento onde maiores valores de WCP foram obtidos nas regiões externas do disco. Esta tendência aumenta com o aumento de WCO. Foi obtida uma diferença significativa entre os valores de WCP nos discos mais quente e frio. Os resultados também indicam que as previsões de WCP considerando a temperatura de ponto quente poderão ser enganadoras, visto que os valores estimados podem ser menos de metade dos calculados em zonas críticas.

Palavras Chave: Transformadores de potência, enrolamento, CFD, teor de água no papel, teor de água no óleo, distribuição de água, transferência de calor

Declaration

I hereby declare, on my word of honour, that this work is original and that all non-original contributions were properly referenced with source identification.

Index

List of Figures

List of Tables

Notation and Glossary

A	Area	m^2
C_p	Specific heat	J kg^{-1} °C^{-1}
k	Thermal conductivity	W m^{-1} °C^{-1}
L	Length	m
Nu	Nusselt number	
Re	Reynolds number	
T	Temperature	°C
P	Perimeter	m
p	Pressure	Pa
r	Radius	m
R	Thermal resistance	°C W^{-1}
v	Velocity	m s^{-1}

Greek Letters

ρ	Density	kg m^{-3}
μ	Dynamic viscosity	Kg s^{-1} m^{-1}

Indexes

cbn	Paper below the copper at part number n
ctn	Paper above the copper at part number n
disc	Disc
ext	External
eq	Equivalent
i	Index or counter
in	Inlet
n	number
out	Outlet
wall	Wall
int	Internal

List of Acronyms

2D	Two Dimensional
3D	Three Dimensional
ACEC	Ateliers de Construtions Électriques de Charleroi
CFD	Computational Fluid Dynamics
DP	Degree of Polymerization
FDS	Frequency Domain Spectroscopy
OD	Directed Oil
ON	Natural Oil
EFME	Empresa Fabril de Máquinas Elétricas
HV	High Voltage
IEC	International Electrotechnical Commission
IEEE	Institute of Electrical and Electronics Engineers
LV	Low Voltage
PPM	Parts per million
PT	Power Transformer
R&D	Research and Development
R&D+I	Research, Development and Innovation
RH	Relative Humidity
THNM	Thermal Hydraulic Network Model
WCO	Water Content in Oil
WCP	Water Content in Paper

1 Introduction

Power transformers (PTs) are complex machines. Since their inception in the nineteenth century, they have become a vital component of the energy distribution grid. Their capability of switching between two different voltages without varying the frequency is essential in electricity transmission. Figure 1 shows a power transformer.

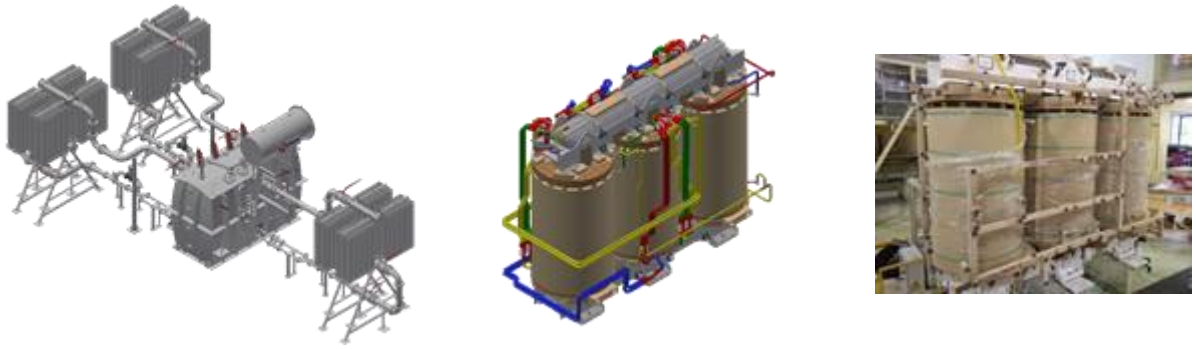

a) b) c)

Figure 1 – Experimental setup (SmarTHER CORE TF) that consists on a three-phase Core type PT: a) Global scheme of the setup; b) 3D scheme of the active part (windings, core and internal connections) and c) photo of the active part. Courtesy of Efacec

The working principle of a PT lies in having two different sets of windings (each for their respective voltage) combined with a magnetic core. As the PT gets energized, an alternating magnetic flux is produced in the core. Through electromagnetic induction the current is transferred from the high voltage winding to the low voltage winding (or vice-versa).

Transformers windings are made up of:

- A conductor, usually copper or aluminium [1];
- Solid insulation, the most used being Kraft paper [1];

During operation, temperature inside a PT rises mainly due to heat produced by conductors and, in some situations, due to the solar radiation [2]. This will accelerate the degradation of the materials. It is important to evaluate which material degrades faster to avoid operating failures. A liquid insulator is used for both electrical insulation and cooling the system. The liquid insulation degrades over time but is easily replaceable, whereas the solid insulation is not. As such, the paper degradation is a topic of upmost importance.

There are several parameters that affect paper degradation. Temperature is the main driving force in solid insulation ageing. It has been concluded that the ageing process is mostly determined by the water content while the ageing rate is mainly influenced by temperature [3].

Most ageing models only take into consideration the temperature effect and as such might not be precise in predicting the lifetime of a PT [4].

1.1 Scope of the Thesis

The determination of water distribution along the winding of a power transformer will be the focus of this work. Through numerical simulation the flow and temperature distribution are predicted, with particular interest in the region of the paper wrapped on discs (discs surface exposed to the liquid insulator). Different approaches to estimate the paper water content were studied. Different operational conditions were also tested on the geometry to see how they influence the temperature and water content in paper (WCP) profiles on the winding. This work is a first analysis to give a better understanding about water distribution in a transformer winding, using tools such as computation fluid dynamics (CFD).

1.2 Efacec – Company Presentation

Founded in 1948 but with its origins in early 20th century, EFACEC is a Portuguese group of companies in the energy, engineering, environment and mobility fields. It was originally known as EFME (Empresa Fabril de Máquinas Elétricas), SARL, and was renamed to EFACEC in 1962 when ACEC (Ateliers de Construtions Électriques de Charleroi) became a major shareholder. Nowadays Efacec Group has several companies located across the globe. It has an international presence in over 65 countries, giving focus in exportations worldwide.

Efacec focuses on three different sectors: Power Products, Systems and Mobility. It currently has more than 220 employees on R&D+I. This work was made in the Power Transformers Research and Development department in Arroteia's facilities, on the Thermal and Fluids Team.

1.3 Work Contributes

Efacec Transformer R&D, namely, the Thermal and Fluids Team, has been focusing their studies on the fluid flow and thermal components inside the PT windings. Additionally, this work was centred in a new research field in the company and yielded new know-how about the water distribution inside a winding. As the presence of water impacts negatively the PT lifespan, it is of great importance for the company to know where the most critical regions will be located and how they can be minimized, as well as how to develop numerical methods to assist the monitoring of the transformer's health. The approaches described in this thesis and the main results builds a pathway to future studies on paper ageing due to water presence and how relevant it is when compared to other causes of ageing like temperature.

1.4 Organization of the thesis

This work is divided in 6 chapters and their subdivisions.

Chapter 1 contextualizes the scope of the work and the main contributes of this thesis.

Chapter 2 presents a literature review on what is known about the topics relevant and what types of studies have been made related to this one.

Chapter 3 describes the problem studied, the software used, the methods chosen and the relevant modeling assumptions considered.

Chapter 4 shows the temperature and WCP profiles obtained and the corresponding discussion of results.

Chapter 5 gives the overall conclusions obtained from this work.

Chapter 6 gives a reflection of what was achieved, and future prospects on this topic.

2 Context and State of the art

The working principal of a power transformer (PT) is electromagnetic induction [1]. It was discovered by Michael Faraday in 1831 [5]. His experiments laid down the basis of what would become known as a transformer. It took mankind 54 years to develop the first reliable commercial transformer [6]. The physical principle has not changed since then, but the machine has been optimized to improve the energy efficiency, reduce manufacturing costs and size [7].

Transformers appeared as a solution to power transmission across long distances. At the time of the transformer inception, direct current (DC) was the main type of current used. By its characteristics, transmission would either require a wire so thick that it would not be practical or having high voltage transmission which is known to be dangerous [6]. DC current transmission also implied that the generating plants had to be near the places where the electricity would be used. Using transformers, alternating current (AC) could be transmitted over long distances using thinner wires with high voltages and then the voltage could be reduced to the one used by the costumer. This had a significant lower cost when compared to the DC alternative.

There are many types of transformers, mainly categorized by their applications. The focus of this work will be on Core-type power transformers, which will be discussed in more detail below.

2.1 Power Transformers

Power transformers are defined as transformers rated 500 kVA or higher [8]. They are used in energy transmission and distribution and operate with the higher voltage range. They can be used to increase (step-up) or decrease (step-down) the voltage in the grid.

2.1.1 Main Components and their functions

PTs main components can be divided into: Tank, Core, Windings, Cooling System, Conservator tank, Bushings [9][10]. The main role and characteristics of the 5 components are:

- Tank: Provides external coverage to all components. Usually made of steel.
- Core: Offers a continuous path to the magnetic circuit flow. Made up of laminated steel sheets to reduce eddy current losses and hysteresis losses [8].
- Cooling System: There are both internal and external cooling mechanisms. External cooling is made with radiators, fans and fins. Internal cooling is done by the liquid insulator.

- Windings: Comprise the electric circuit. Responsible for changing the voltage. PT have primary windings and secondary windings, depending on their input and output. The windings with higher voltage are called high voltage windings (HV) while the windings with lower voltage are called low voltage (LV) windings. Copper is frequently chosen as the material since it has high conductivity and high ductility.
- Conservator tank: Responsible to add extra space to the PT when oil expands.
- Bushings: Are responsible of transmitting electric power in and out of the transformer tank [1].

The PT components with more relevance to this study are the windings as they are the location in which the water migration phenomena will be most prominent. As such, it is important to mention their materials and properties. The winding is composed of copper/aluminium discs wrapped in paper (Figure 2), who acts as a dielectric insulator [1]. These discs heat up during the PT operation. Fluid flows through the winding channels and acts as coolant and as an insulator. Washers are used to direct fluid to the hottest spots in order to maximize the heat removal of the equipment. Figure 2 shows a Core type PT winding scheme.

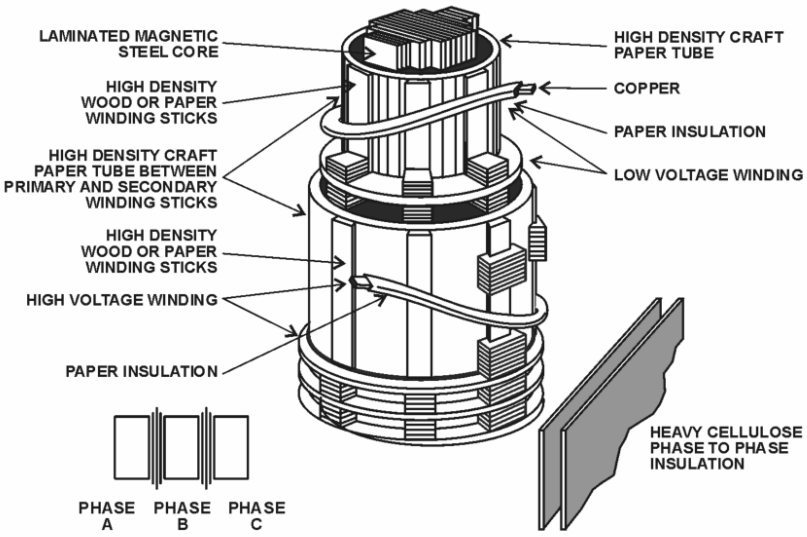

Figure 2 - Core-type power transformer winding scheme. Taken from [8]

Copper

Copper is the main choice for conductors because of its ability to conduct electricity, high ductility, elevated temperature tolerance and abundant quality [11], [12]. Copper losses occur due to the resistance of the primary winding to the magnetizing current [8], generating heat that needs to be removed, otherwise the paper wrapped in the copper and oil degrades faster and compromises the transformer's lifetime. This is the reason why the liquid insulation works as a coolant. The liquid insulator travels through the windings and refrigerates the copper windings. It then exits the main transformer body through the top, goes through external cooling and reenters at the bottom, making a closed loop system.

Paper

Paper and pressboard represent the solid insulation inside a transformer [1]. They comprise different parts that have distinctive properties such as thickness or density, which are properly chosen according to their application. The basis of paper is cellulose, which is a natural polymer made up of a chain of D-glucose rings, as shown in Figure 3 [13].

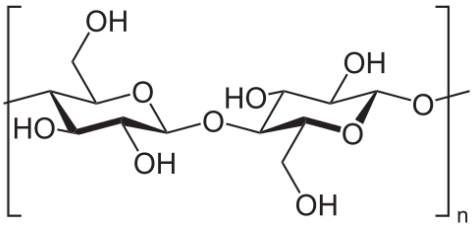

Figure 3 - Cellulose molecular structure. Taken from [14]

Paper is crucial in keeping the dielectric integrity of a transformer. However, it is not easily replaced like the liquid insulation (paper is located in several places of difficult access, Figure 2). Besides, the paper deteriorates over time due to temperature, moisture content and other factors. While the temperature is mainly responsible for the ageing rate, moisture content will influence the ageing process [15]. As such, the main cause of a transformer malfunction is due to the degradation of paper by its ageing. For that reason, it is of great interest to analyze several factors that contribute to paper deterioration and to study solutions that minimize paper wearing.

A good indicator of paper degradation is considered to be the degree of polymerization (DP) value. While this value can be directly measured from a sample, the PT operation procedures make it impossible to obtain a sample without stopping it and disconnecting it from the grid, which is not desirable. Indirect measurements of DP are used as an alternative [16].

The DP value for new paper is approximately 1200 [17]. Around the 200 DP mark it is considered that paper has reached the end of life [18]. The decrease in DP value is caused by

ageing processes like oxidation, hydrolysis and pyrolysis , which would be discussed in more detail in section 2.2.1 [19].

When a transformer is energized some energy will be lost in the form of heat. The paper in windings will be the first resistance to this heat dissipation. The locations with the higher temperature are called hot spots and are critical parts of paper degradation in a transformer.

The paper is one of the components of solid insulation of a PT. The solid insulation divided into two main components: a thin component divided into the winding insulation and the thin barriers, and thick insulation, which is responsible for a third to half of the solid insulation weight [20].

Oil

Usually provided by a mineral oil, but there are alternatives like organic esters and silicone liquids [21]. It has two main functions: it works as an electrical insulator and as a heat dissipation mechanism [1]. Oil fills up the entirety of the tank and by its circulation inside the transformer, receives the heat generated by the various power losses. PTs have an external cooling component to compensate for the increase of temperature inside the tank, letting the oil reenter the PT with a lower temperature. It is important that the oil has a high flash point value, to avoid vapor formation [21]. Oil is generally hydrophobic, but with its ageing the amount of polar components increase, allowing more bonds with water molecules [22].

Another important function of oil is can be used to indicate the conditions of the PT [1], and through periodical examinations to the oil, the PT can be monitored. There are designated sample points in which oil can be retrieved and tests can be performed. Further details are shown in section 2.3.1.

2.1.2 Types of Power Transformers

PTs are mainly divided into two types, based on its structure: Core and Shell (Figure 4). They have several differences, the main one being the conformation between the windings and the magnetic core. Core-type power transformers have the windings around the magnetic core while Shell-type have the core surround the windings. This work focuses exclusively on core type transformers.

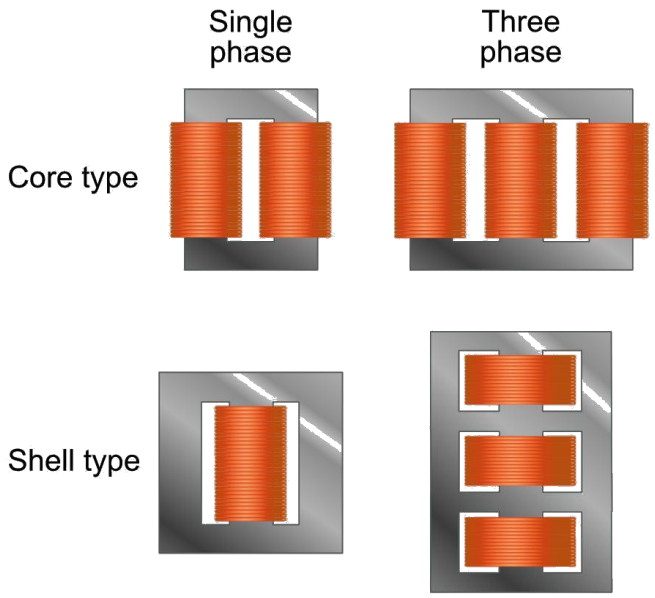

Figure 4 - Shell vs Core Power Transformer. Taken from [23] *[Legend: winding represented by orange and core by gray]*

Oil-immersed PTs can also be classified according to their cooling method. The nomenclature uses a 4-letter code, where the first two specify the internal cooling that contacts with the windings, while the last two refer the external cooling. For each pair of letters, the first one indicates the medium while the second identifies the mechanism of cooling [24]. The different nomenclatures that exist are shown in Table 1.

Table 1 - Cooling class letter descriptions. Taken from [1]

		Code Letter	Description
Internal	First Letter (Cooling medium)	O	Liquid with flash point less than or equal to 300 °C
		K	Liquid with flash point greater than 300 °C
		L	Liquid with no measurable flash point
	Second letter (Cooling mechanism)	N	Natural Convection through cooling equipment and windings
		F	Forced circulation through cooling equipment, natural convection in windings
		D	Forced circulation through cooling equipment, directed flow in main windings
External	Third Letter (Cooling medium)	A	Air
		W	Water
	Fourth letter (Cooling mechanism)	N	Natural convection
		F	Forced convection

The transformer chosen for analysis has an ODAF nomenclature (Table 1).

2.1.3 Problems Associated

PTs are known to have high efficiency values (99.5 % or greater) [1]. Generally speaking, the efficiency of a PT decreases when the load increases, as losses caused by the load increase. These losses produce heat in certain regions that can be detrimental to the PT failure. The location of these areas is important when idealizing the cooling of the PT [25]. The higher the temperature, the faster paper degrades. Water has also a role in paper degradation. It can infiltrate the transformer tank, increasing the water content in paper (WCP) and water content in oil (WCO). In situations where temperature is abnormally high, the formation of gas bubbles may occur [26]. These reduce the dielectric strength and may cause partial discharges, compromising the dielectric integrity of the PT. [27]

2.2 Limiting factors in power transformers' lifetime

From the manufacturing process of a PT to the end of its lifespan, components are slowly but irreversibly degrading. An analysis of the main causes of degradation of the solid and liquid insulations are described in the following sections.

2.2.1 Solid Insulation - Paper

The paper insulation is the most critical component of the transformer when talking about material ageing, since it cannot be replaced, in opposition to the oil, which can be easily replaced. As such, it is important to understand what the main causes of paper ageing are. There are internal and external factors that accelerate its ageing. The main external factors are temperature and water, but there are other factors like pH and light, among others. [3]. The acidity of paper is the most important internal factor.

Cellulose ageing processes occur simultaneously and contribute to the increase of each other (oxidation, hydrolysis and pyrolysis), making the modeling of this processes a complex task [16].

Temperature

The main cause of thermal degradation of cellulose are the chemical reactions caused by hydrolysis and oxidation. Above 130 °C pyrolysis becomes the main degradation mechanism [16]. A temperature increase translates in an increase of the reaction rates. Harlow defends the rule of thumb that says that "for every 10 °C rise in temperature, reaction rates double". However, Erhardt et al. contradict this conclusion, claiming that it does not apply to paper and the value is actually lower, being as low as 5 °C [3].

Water

Water plays several roles in cellulose degradation. It is a reactant in acid hydrolysis, it serves as a swelling agent, which increases the surface area for reactions [3]. The presence of water decreases the dielectric strength. In general, the mechanical life of cellulose insulation is reduced to half by doubling the water content [28].

pH

Acidity increases the degradation of cellulose by the acid-catalyzed hydrolysis. Deacidifying paper will result in a slower ageing [3].

Light

Is important in natural ageing of paper. Light exposure creates free radicals, giving rise to the photooxidation of cellulose [3]. This effect is not verified in PT, as the cellulose is inside the tank.

The three most predominant reactions of paper degradation are:

Oxidation

Oxygen can promote chain scission. Oxidized cellulose degrades faster than normal cellulose. It is the primary reaction below 60-75 °C [16]. Increases the acidity in the medium [3]. Sub-products: CO, CO_2 and H_20.

Hydrolysis

The main degradation process of natural ageing [3]. Causes random chain scissions at random positions. It is acid catalyzed, so oxidation contributes heavily. It is predominant in the range 70-130 °C [16]. Products: H^+, CO, CO_2

Pyrolysis

Is produced exclusively by heat. It is the main degradation process above 130 °C [16]. If temperatures go beyond 140 °C, the reaction becomes self-accelerated and generates water and oxygen (promoting the effects of oxidation).

2.2.2 Liquid insulation - Oil

Transformer oil is subjected to oxidation. Oil oxidation produces several components, the main two being carbon dioxide and water. Oxidation increases the acidity of the oil. High levels of acid can cause sludge formation in the oil, affecting the heat dissipation [1].

Temperature has also influence of the oil degradation. An increase of 8 to 10 °C approximately doubles the degradation ratio of transformer oil. The degradation of oil produces by-products that affect both oil and paper degradation [26].

The presence of water in oil has a negative impact on the material dielectric properties [26]. With oil ageing the oxidation causes an increase of chemical agents to which water can bond [29].

To minimize the ageing of paper insulation caused by the oil degradation processes, the PT can be submitted to several drying processes [29]. Most of them either won't remove much water in paper (Hot oil circulation), while those who do it might imply the removal of the PT from the energy grid (Low frequency heating). Other technologies like a stationary molecular sieve have been developed to avoid the down time of the transformer when removed from operation [29].

2.3 Water Dynamics

Water migration is a slow process [30]. It can be activated by concentration, temperature and pressure gradients [20]. Concentration gradients will be more predominant during transformer repairing and oil replacement. Pressure gradients are the most important mechanism on the drying process. Finally, temperature gradients are the key factor for water movement under regular operation conditions. As temperature increases, water will move from paper to oil, and vice-versa[31]. The typical known profiles of temperature and water distribution along the winding are shown in Figure 5.

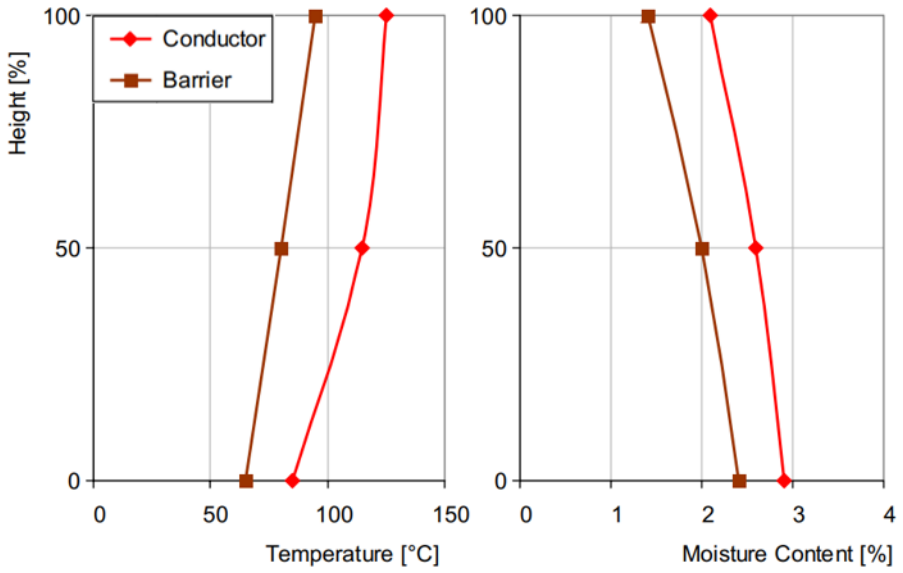

Figure 5 - Distribution of temperature and water content in the conductor and barrier insulation of a winding. Adapted from [32]

It is expected that paper insulation at the bottom of the windings has more water content than the top, while the temperature has the opposite profile.

The assessment of the water physical state inside the windings is not clear. In reality, water can exist in paper in four different states: adsorbed on the surfaces, free water in the capillaries, imbibed free water and vapor [22]. Paper contains much more water than oil [22]. Water migrates into cellulose by sorption, which includes both adsorption and absorption. Water desorption in paper is faster than adsorption [20].

Paper, being a fibrous material, is made up by fibers and air-filled voids. It shows high resistance to water diffusion [33]. As such, it is considered that the thick insulation does not contribute in water migration as the diffusion time constant has a large value [20]. Paper degradation also affects its water sorption capabilities. Aged paper has less water absorption capabilities than new paper [34].

Water in oil can exist in three different states: water dissolved in oil, water bound to oil molecules and free water in suspension when the solubility of oil is exceeded (the oil is saturated) [22].

Water solubility in oil can be expressed using equation 1 [22].

$$\log x_w^s = A - \frac{B}{T} \tag{1}$$

where x_w^s is the saturation solubility of water in oil in ppm and A and B are coefficients that have been defined by different authors, as show in Table 2.

Table 2 - Different estimated coefficients A and B for the Arrhenius form of equation 1 of the solubility of water in oil. Taken from [22]

	Oommen	Griffin	Shell
A	7.42	7.09	7.30
B	1670	1567	1630

Using equation 1 it is visible that water solubility in oil increases with an increase in temperature.

During the manufacture of the PT the cellulosic insulation is dried, and it is expected that after the final assembly the water content in paper is less than 0.5 to 1.0 % [32]. However, the amount of water inside the PT increases with time. This is due to the water ingress from moisture from the atmosphere and water generated from the decomposition of insulating materials [32].

2.3.1 Methods of determination of water content in paper

There are direct and indirect methods of the water content in paper (WCP) determination [22]. Direct methods are invasive and require a sample of paper, which is only obtainable by shutting down the PT and removing it from the grid. Indirect methods can be a good alternative, however the values of WCP obtained will simply be estimations.

There are some estimation techniques to measure WCP on a PT indirectly. While recent ones have emerged like frequency domain spectroscopy (FDS) and the use of monitoring sensors that measure useful properties like water activity (that can be converted in water content in oil, WCO) [35], the traditional method of WCP estimation consists in obtaining a sample of oil from the PT and using the Karl Fischer titration to determine the WCO. Then, with the auxiliary of the equilibrium curves an estimation of WCP in the windings can be obtained.

Karl Fischer titration

Developed in the 1930s, the Karl Fischer titration uses a special reagent made up of iodine, sulfur oxide, a base and a solvent such as alcohol that reacts specifically with water [32]. The Karl Fischer titration can be volumetric or coulometric. The determination of water content in paper using the Karl Fischer coulometry is described in IEC 60814.

Despite being considered a valid method of WCP estimation, the accuracy of this method has some intrinsic compromises. First, the sample of oil ingresses water from the moment it is retrieved from the PT until it arrives at the laboratory for analysis. Oil additives and ageing byproducts can also influence the measured value [32]. Water molecules have different types of bonds (hydrogen and Van de Waals bounds) which require different levels of energy to be broken. Different reaction times and temperatures might influence the results obtained.

Equilibrium curves

There have been a few attempts in representing the equilibrium of water in oil/paper systems. The first report of equilibrium curves for these systems was done by Fabre and Pichon in 1960. They used Kraft paper and used the Karl Fischer method to determine the water content in oil and in the oil-impregnated pressboard [22].

In the decade of 1980, Oommen created a new set of equilibrium curves. Combining the Moisture in Oil vs Relative Humidity curves in air with Moisture in Paper vs Relative Humidity he obtained the Moisture in Paper vs Moisture in Oil equilibrium curves, shown in Figure 6. Griffin et al. also developed other set of curves using the same method as Oommen's. However, they used a formula created by Fessler et al that had an error.

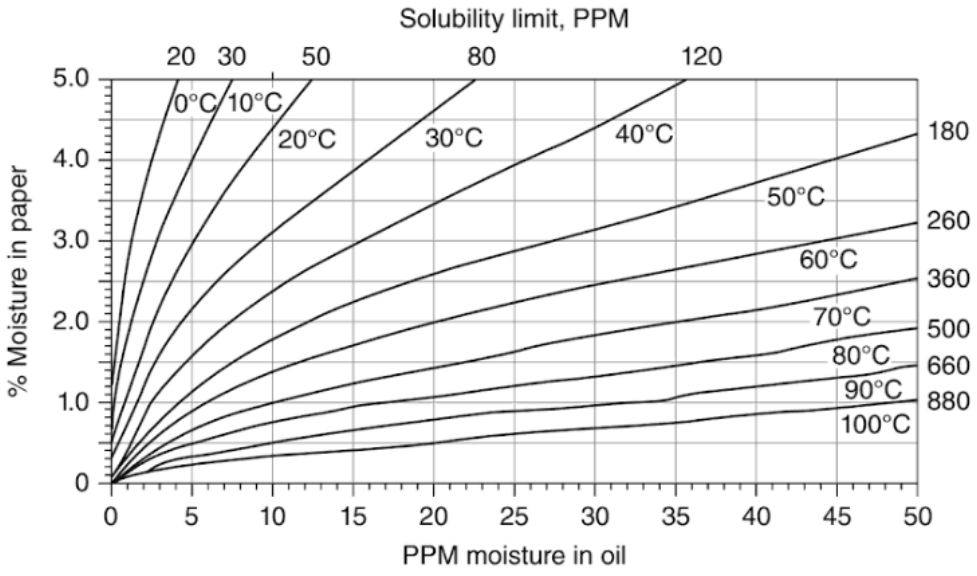

Figure 6 – Oommen's curves of moisture equilibrium for paper-oil systems. Taken from [21]

Figure 6 shows Oommen's equilibrium curves for different temperature values. The water content in oil is measured in parts per million (PPM) while the water content in paper is measured in the weight of water in paper divided by the weight of the dry paper. More recently, MIT expanded the equilibrium curves up to 800 ppm of water in oil.

As the name suggest, these curves are only valid for equilibrium conditions, which are rarely obtained during the PT operation.

2.4 Numerical methods

2.4.1 Computational Fluid Dynamics

Computation Fluid Dynamics (CFD) provide a new approach to study and understand the physical events and how fluid flows behave in geometries of interest [36]. CFD simulations on power transformers have been used in recent years, focusing on the flow and thermal studies on the windings [37]–[39].

The numerical methods applied in CFD involve the solving of partial differential equations, which introduces some deviations to the results. A special care to parameters like stability, convergence and consistency is needed, otherwise the results obtained may not translate the reality [36]. Depending on the complexity of the phenomena studied, the geometry applied, the steady-state vs transient approach and accuracy pretended, the computational resources needed can be high and simulation times can be extensive [40]. For these reasons, other alternatives might be more appealing.

2.4.2 Thermal Hydraulic Network Models

Thermal Hydraulic Network Models (THNMs) are an alternative to CFD that have lower time-to-solution but use simpler algebraic equations that use analytical and/or empirical coefficients [40]. They use the same physical principles of mass, momentum and energy conservation. THNMs consider an ideal mix flow, so the analysis is more based on average values [41]. THNMs have been developed and compared with CFD model the temperature and flow distribution in PT windings [40]–[42].

3 Formulation of the transfer model

3.1 Problem description

The main objective of this work is to analyze the water distribution along a power transformer. The winding is the part of the PT chosen to be studied because it has a significant amount of cellulose and is where most water migration occurs at faster ratings [32]. Paper in the windings is highly degraded not only by the elevated temperatures that are caused by the heat losses, but also for the presence of water retained in the paper [3].

A 2D axisymmetric model (Figure 7a) of a winding was chosen to better represent the Core-type winding cylindrical geometry (Figure 2). As the PT gets energized, the winding will heat up. The oil enters through the bottom and travels upwards. Washers are used to make the fluid change direction, which consequently increases the cooling of the discs. Each section between two washers is called a pass (Figure 7b). There are several arragements possible for the number of discs and passes in a transformer winding. These vary to respect electrical and mechanical aspects as well as thermic aspects, to avoid the reach of critical temperatures. In this work the analysis of the water distribution in the papers covering the discs were carried out using numerical simulations.

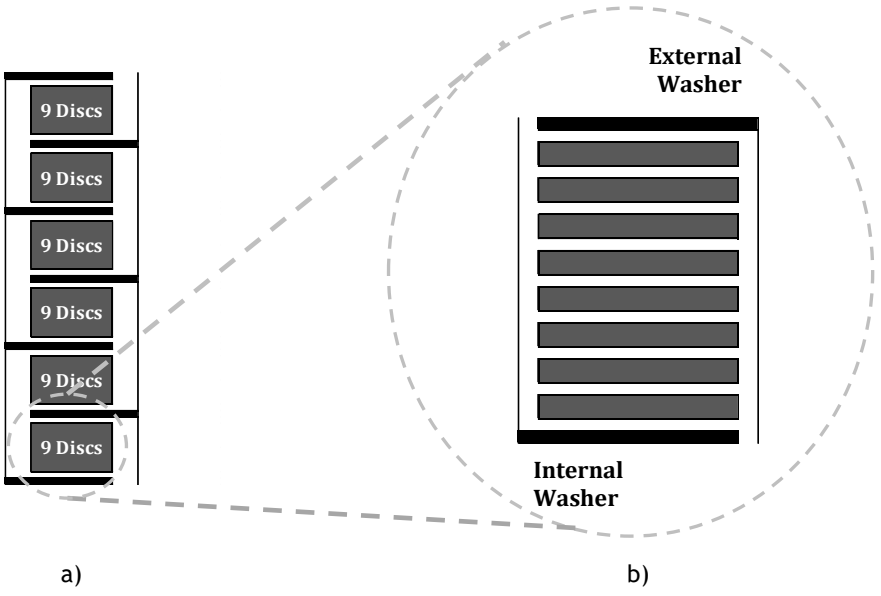

Figure 7 – a) Winding Scheme; b) - 1st Pass Scheme

3.2 Distribution of paper water content in a pass

The first analyzes considered only the first pass of the winding (Figure 7b) to study the flow and temperature distribution inside the pass, with particular interest in the region of the paper wrapped on discs (discs surface exposed to the oil). Different methods to estimate the paper water content were studied.

3.2.1 Geometry Dimensions

A scheme of the pass (Figure 8a) used for the simulations and its dimensions (Figure 8b) were provided by Efacec.

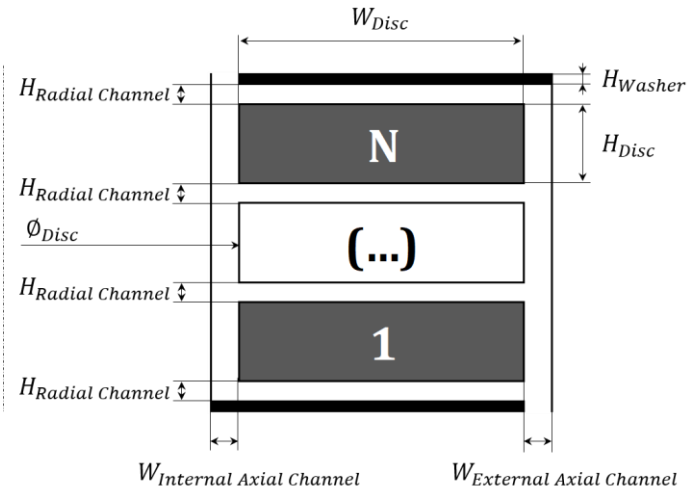

a)

Dimensions / mm	
$\emptyset_{Disc}$	735.00
H_{Disc}	17.30
W_{Disc}	58.14
H_{Washer}	2.00
$W_{(Internal\ Axial\ Channel)}$	6.00
$W_{(External\ Axial\ Channel)}$	6.00

b)

Figure 8 - a) Winding's pass scheme; b) Winding dimensions

Radial channels (horizontal direction, Figure 8a) have different heights. In the pass they all are 3 mm high except for the second one counting from the bottom, which is 4 mm high.

ANSYS® SpaceClaim was used to build a pass geometry with 9 discs (as shown in Figure 9a). The fluid domain is represented by the blue color, while the solid domain (paper + copper) is represented by pink. The nomenclature used in the results and discussion section is represented in Figure 9b. An extended channel was introduced in the outlet (Figure 9a) to avoid reverse flow.

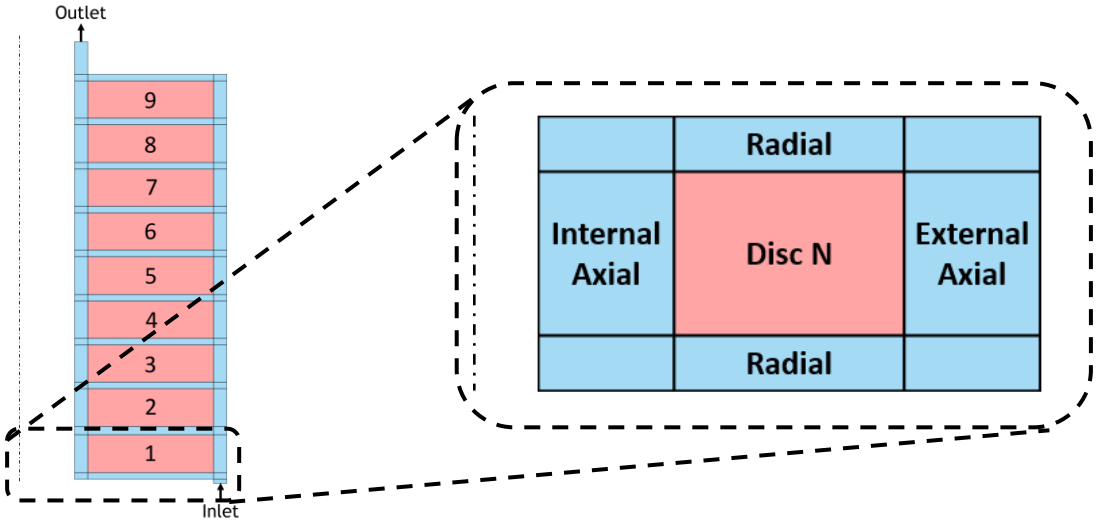

Figure 9 - a) Winding's pass with 9 discs; b) Nomenclature used in thermal analysis

In Figure 9a, the dashed line represents the radial symmetry. The disc wall nomenclature is similar to the one in Figure 9b.

The oil velocity inside the winding should be set with caution, since for scenarios where the Reynolds number inside the winding exceeds 1000, static electrification of the insulation may occur, which may result in partial discharges [43]. To avoid the aforementioned problems the Reynolds number were calculated for each simulation tested.

The calculation of the inlet and outlet flow rate considered that the inlet and outlet areas (*A*) were calculated by equation 2 obtained for ring areas (axisymmetric model, Figure 9a)

$$A = \pi * ({r_{ext}}^2 - {r_{int}}^2) \quad (2)$$

The internal and external radius (r_{int} and r_{ext}, respectively) are presented in Table 3.

Table 3 - Internal and external radius for the pass inlet and outlet

	Inlet	Outlet
r_{ext} / m	0.432	0.367
r_{int} / m	0.426	0.362
A / m^2	1.62×10^{-2}	1.14×10^{-2}

3.2.2 Transfer model

The two-dimensional model considers the heat generated by 9 discs of a pass (Figure 9a) and the heat exchanged between the discs and the oil that flows inside the pass. The

temperature distribution inside the pass (discs and oil domains, Figure 9a) was obtained in steady-state. The commercial CFD package ANSYS® *Fluent* 18.1 was used.

The oil and discs properties as well as the boundary conditions and the numerical procedure are described below.

The water content of the paper that covers the discs (Figure 10a) was estimated considering the temperature distribution obtained in steady-state. Further details are presented in section 3.3.2.4.

Oil and discs (paper and copper) properties

The oil used for this study was Nynas® Nytro Taurus. The properties needed for simulation are the density (Equation 3), specific heat (Equation 4), thermal conductivity (Equation 5) and dynamic viscosity (Equation 6). All of them vary with the temperature. The following equations were provided by the respective supplier. The density ρ can be obtained using:

$$\rho = 1065.801 \ - 0.6585 \times (T + 273.15) \tag{3}$$

where T is temperature in °C and the density units are kg m^{-3}.

The specific heat $C_p$can be obtained using:

$$C_p = 844.5521 + 3.483425 \times (T + 273.15) \tag{4}$$

where T is temperature in °C and the specific heat units are J kg^{-1} °C^{-1}.

The thermal conductivity k can be obtained using:

$$k = 0.1562308 - 0.00007857143 \times (T + 273.15) \tag{5}$$

where T is temperature in °C and the thermal conductivity units are W m^{-1} °C^{-1}.

The dynamic viscosity μ can be obtained using:

$$\ln \mu = -20.04413 + 12078.37 \times (T + 273.15)^{-1} - \\ -4122209 \times (T + 273.15)^{-2} + 574840600 \times (T + 273.15)^{-3} \tag{6}$$

where T is temperature in °C and the dynamic viscosity units are kg m^{-1} s^{-1}.

The aforementioned properties were implemented in the solver as UDF functions (i.e. User Defined Functions).

The oil was considered to be a Newtonian and an incompressible fluid.

The winding discs (Figure 9a) are composed by copper conductors wrapped by Kraft paper. Figure 10a shows the HV disc conformation where the copper and the paper are the red and white regions, respectively, and Figure 10b shows their dimensions.

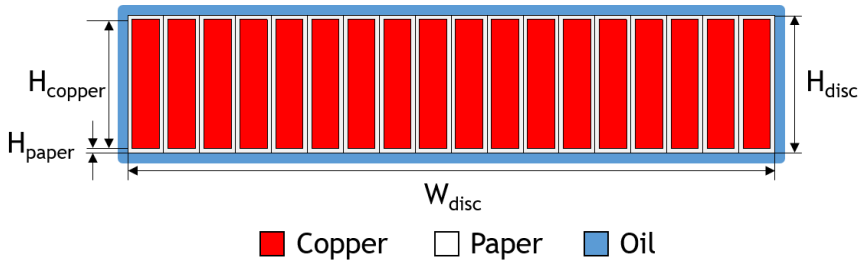

a)

Dimensions / mm	HV
H_{Disc}	17.30
W_{Disc}	58.14
H_{Paper}	0.70
H_{Copper}	15.60
W_{Copper}	1.83

b)

Figure 10 - a) HV disc scheme; b) HV disc dimensions

The uniform distribution of copper and paper in the radial and axial direction (vertical and horizontal direction in Figure 10a, respectively) can be modeled as a uniform material with an equivalent radial and axial thermal conductivity [40]. Further details are shown in Appendix 2. The equivalent material considered has a radial and axial thermal conductivity of 0.37 and 1.18 W m-1 °C-1, respectively.

The paper that wraps the copper and is located at the limits of the disc (Figure 10a) is directly exposed to the oil (represented by the blue color in Figure 10a). During the winding operation, the water can migrate between the oil and this exposed paper. For that reason, focus was given to the surface of the discs.

Boundary conditions

The boundary conditions considered for the pass simulation are shown in Table 4.

Table 4 - Boundary conditions set in the pass inlet, outlet and walls

Boundary Type	Momentum			Thermal	
	Boundary Condition	v_0 / m s^{-1}	P_0 / Pa	Boundary Condition	T_0 / °C
Inlet	Velocity	0.10	-	Temperature	30
Outlet	Pressure	-	0	-	-
Pass Wall	No slip	-	-	Adiabatic	-
Disc Wall	No slip	-	-	Coupled	-

All the walls (of the pass and of the discs) were set with a non-slip condition. The heat continuity between the inner and outer side of each disc was ensured by considering a Coupled boundary condition [44]. The pass walls were considered adiabatic. Data for velocity and temperature inlets was considered based in the typical range of an Efacec OD type PT. The

minimum velocity are the values of a ON (as shown in Table 1) type PT and the maximum velocity is one that the Reynold number inside the geometry does not exceed 1000. The minimum temperature is the ambient temperature and the maximum temperature at the inlet should be one that after going through the transformer, the fluid temperature must be below its flash point (for the oil studied, 135 °C [45]).

The Reynolds number can be given by Equation

$$Re = \frac{\rho \, v \, D_h}{\mu} \tag{7}$$

where ρ is the density in kg m^{-3}, v is the velocity in m s^{-1}, D_h is the hydraulic diameter in m and μ is the dynamic viscosity in kg m^{-1} s^{-1}. The hydraulic diameter of an annulus is equal to $2\,(r_{int} - r_{ext})$. Using Equation 3 and 6 at 30 °C (condition used for the simulation, Table 4), the Reynolds number for the velocity at the inlet (0.10 m s^{-1}, as shown in Table 4) is equal to 86.6.

A constant energy source term was added to each disc to represent the heat losses (Table 5). The values were provided by Efacec and were obtained from FEM simulations coupled with proprietary tools from the company. Disc 1 has the highest heat source, while discs 6 and 7 have the lowest heat sources.

Table 5 - Heat source of each disc

Disc number	Volumetric heat source / W m^{-3}
1	215 051
2	185 127
3	173 158
4	167 971
5	165 976
6	165 577
7	165 577
8	166 375
9	167 173

As steady state was considered, water transport can be determined through the Oommen's equilibrium curves (Figure 6, section 0)

Numerical Procedure

Numerical simulations were performed using the commercial CFD package ANSYS® *Fluent*. The mesh was created using ANSYS® Meshing. A number of mesh elements of 435 662 were used (found adequate to ensure grid-independent results, appendix 1.2).

Gravity was considered with value of -9.8 m s^{-2} in the same direction of the axis of symmetry. The Navier-Stokes equations were solved assuming laminar regime using the Coupled

scheme [44]. The momentum and energy equations were discretized by the Second Order Upwind scheme [44] and the pressure equation by the PRESTO! scheme [44]. The Standard Initialization was chosen [44]. The convergence criterion was that the scaled residuals were below 10^{-6} and 10^{-9} for the continuity equation and the energy equation, respectively.

Assumptions considered to calculate the paper water content

Steady-State was considered for the simulations. This is rarely achieved during the PT operation, because the energization (disc heat source) changes over time, leading into a dynamic behavior of the temperature and water content [29]. The closest results would be obtained considering an equilibrium through long time. Nevertheless, this type of approach gives the locations where the paper will have higher concentration of water and where problems associated with the water content occur [29].

In steady-state the water present in oil is in equilibrium with the water retained in paper for a specific temperature of the system. Therefore, the water content in paper (WCP) can be calculated through the moisture equilibrium curves (Figure 6) for knowing values of water content in oil (WCO) and paper temperature. The water content in oil was assumed equal to the inlet value and uniform along the pass (the water in paper and in oil are in equilibrium and for that reason there is no mass exchange between paper and oil). The paper temperature (e.g. temperature distribution along the disc surface) was calculated through CFD simulations.

This analysis neglects the water formation in the paper, however the effect of a change in WCO in WCP was analyzed by considering different values of WCO at the inlet. An average value of water content was calculated in the direction of the paper thickness, i.e does not consider a gradient of water content inside the paper. It also does not consider the migration of water from the winding walls to the oil circulating as the diffusion time in the winding walls is much higher when compared to the disc walls [32]. It also does not consider a finite amount of oil inside the transformer.

Data from the moisture equilibrium curves was extracted from Figure 6. To be able to determine the WCP for a given WCO, a series of linear interpolations were made.

Different values of temperature were studied to estimate the paper water content: i) maximum temperature out of all disc surfaces, also known as the hot spot temperature, ii) average temperature of the disc surface, iii) average temperature of each disc surface and iv) temperature distribution of paper wrapped on discs. The reasoning behind these approaches is that i) is often used in thermal analysis, ii) could be implemented in a THNM, while iii) gives a more detailed look of the WCP and iv) represents with the most accuracy of them all the steady-state scenario of water distribution in the paper.

In future analysis where the water migration should be studied in the transient regime, the water diffusion through the paper should be consider, which increases the mathematical model complexity and can imply a huge computational cost with higher time-consuming simulations. To balance these implications some the complexity of geometry should be readjusted (as made in THNMs [41]) and values like the ones obtained in iii) should be taken into consideration.

The IEC 60814 norm states that the WCO at the loading of a PT must be below 10 ppm [46]. The IEEE Std. C57.106 st

ates that, for a typical PT, the WCO is suggested to be kept below 20 ppm [47]. If this value is exceeded, the transformer should stop operating to renew the oil. The analysis of water distribution was made for a WCO at the inlet of 5 ppm, 10 ppm and 20 ppm.

3.3 Distribution of paper water content in a winding

The whole winding was considered, and a parametric analysis was performed. Different conditions were tested on the geometry to see how they influence the temperature and WCP profiles on the winding.

3.3.1 Geometry dimensions

The winding is made up of 6 passes, as shown in Figure 7a. Each pass the same dimensions as the ones shown in Figure 8b, the only difference being different heights for the radial channels. Table 6 shows the heights of the radial channels.

Table 6 - Distribution of the radial channel heights on the winding

Radial Channel	Channel Height / mm					
	Pass 1	Pass 2	Pass 3	Pass 4	Pass 5	Pass 6
10	3	3	3	3	3	3
9	3	3	3	3	3	4
8	3	3	3	3	3	4
7	3	3	3	3	3	4
6	3	3	3	3	3	4
5	3	3	3	3	3	4
4	3	3	3	3	3	4
3	3	3	3	3	3	4
2	4	3	3	4	4	4
1	3	3	3	3	3	3

The discs have the same dimensions and are equal to the ones shown in Figure 8b.

3.3.2 Transfer model, boundary conditions and numerical procedure

Four different simulations were run. One of them has the same boundary conditions as the ones chosen for the simulation in a pass (section 0). In the other three a parameter was varied. The parameters chosen were velocity at the inlet, inlet temperature and the disc losses. Table 7 represents a scheme of the cases chosen. From simulation 1 to 2 the velocity was doubled (from 0.1 to 0.2 m s^{-1}). From simulation 1 to 3 the temperature at the inlet increased 10 °C (from 30 to 40 °C). From simulation 1 to 4 the disc heat sources were doubled (Table 8)

Table 7 – Simulations made for the parametric analysis of the winding

Simulation	1	2	3	4
Inlet Velocity	v_1= 0.1 m s^{-1}	v_2= 0.2 m s^{-1}	v_1= 0.1 m s^{-1}	v_1= 0.1 m s^{-1}
Inlet Temperature	T_1 = 30 °C	T_1 = 30 °C	T_2 = 40 °C	T_1 = 30 °C
Disc heat source	Set 1	Set 1	Set 1	Set 2

The different sets of disc heat source can be found in Table 8.

Table 8 – Sets of disc heat source used in the simulations

Pass	Disc number	Set 1 W m^{-3}	Set 2 W m^{-3}	Pass	Disc number	Set 1 W m^{-3}	Set 2 W m^{-3}
	1	215 051.0	430 102.0		28	166 375.3	332 750.5
	2	185 127.4	370 254.8		29	165 976.3	331 952.6
	3	173 158.0	346 315.9		30	165 976.3	331 952.6
	4	167 971.2	335 942.4		31	166 375.3	332 750.5
1	5	165 976.3	331 952.6	4	32	165 976.3	331 952.6
	6	165 577.3	331 154.6		33	165 976.3	331 952.6
	7	165 577.3	331 154.6		34	165 976.3	331 952.6
	8	166 375.3	332 750.5		35	165 976.3	331 952.6
	9	167 173.2	334 346.5		36	165 976.3	331 952.6
	10	165 577.3	331 154.6		37	167 572.2	335 144.4
	11	165 577.3	331 154.6		38	166 774.3	333 548.5
	12	165 976.3	331 952.6		39	166 774.3	333 548.5
	13	165 976.3	331 952.6		40	166 375.3	332 750.5
2	14	166 375.3	332 750.5	5	41	166 375.3	332 750.5
	15	166 375.3	332 750.5		42	165 976.3	331 952.6
	16	166 774.3	333 548.5		43	165 976.3	331 952.6
	17	167 173.2	334 346.5		44	165 577.3	331 154.6
	18	167 971.2	335 942.4		45	165 976.3	331 952.6
	19	165 976.3	331 952.6		46	167 173.2	334 346.5
	20	165 976.3	331 952.6		47	166 375.3	332 750.5
	21	165 976.3	331 952.6		48	165 577.3	331 154.6
	22	166 375.3	332 750.5		49	165 577.3	331 154.6
3	23	166 375.3	332 750.5	6	50	166 375.3	332 750.5
	24	166 375.3	332 750.5		51	168 370.2	336 740.4
	25	166 375.3	332 750.5		52	173 158.0	346 315.9
	26	166 375.3	332 750.5		53	185 127.4	370 254.8
	27	166 375.3	332 750.5		54	215 849.0	431 698.0

The values of set 2 in Table 8 are the values of set 1 doubled. The highest value is reached in discs 7, 10, 11, 44, 48 and 49 (165 677.3 and 331 154.6 for set 1 and 2, respectively). With exception to the Xnumber of mesh elements, the numerical procedure and the assumptions considered to calculate the paper water content are identical to the ones in section 3.2.2, respectively. A number of mesh elements of 2 607 414 were used for the winding simulations (found adequate to ensure grid-independent results, appendix 1.2).

4 Results and discussion

4.1 Distribution of paper water content inside a pass

Figure 11 shows the velocity magnitude distribution inside the pass with 9 discs (Figure 9a). The oil enters the pass at the bottom with an uniform velocity (0.10 m s^{-1}, Table 4), flows through the external axial channel (Figure 8a) and it heterogeneously distributes through the channel, exiting the pass with an average velocity of 0.14 m s^{-1} (i.e. this outlet condition is the inlet conditions of the next pass of the winding). The heterogenous distribution is evident in Table 9.

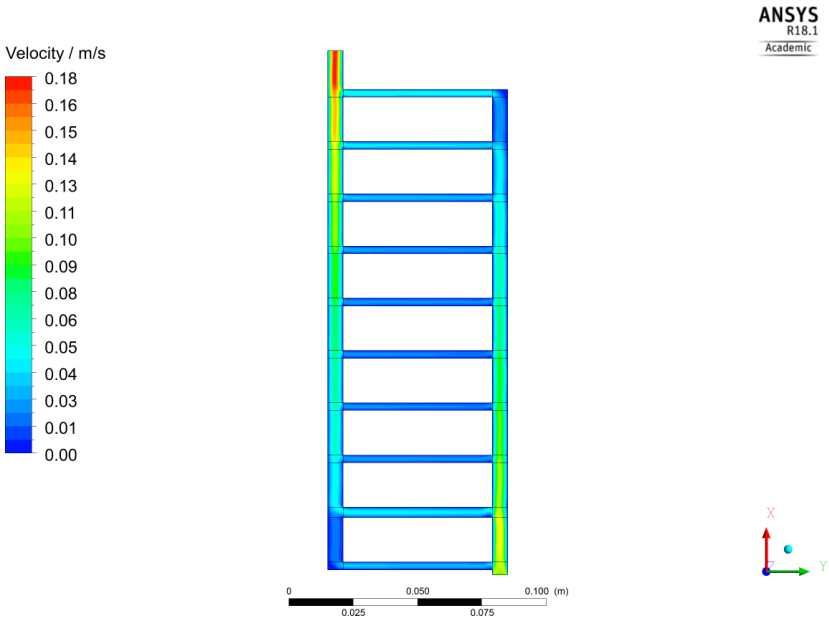

Figure 11 - Velocity magnitude distribution inside a pass with 9 discs (Figure 9a)

Table 9 shows the flow rate distribution in the pass channels (absolute and percentage values). The percentage of fluid distribution varies between 6 and 17 % and the channels with the higher percentage of fluid (i.e. higher than 10 %) are the first two channels (channel 1 and 2) and the last 3 channels (channel 8, 9 and 10). The channels with lower percentage of fluid (i.e. lower than 10 %) are located in the middle of the pass (channel 3 to 7). This heterogeneous division of the fluid clearly contributes to a consistent variation of the oil and discs temperature along the pass (Figure 12a and b, respectively). The hottest discs have the higher value of heat source (discs 1 and 2, Figure 12b; Table 5)

Table 9 - Flow rate distribution inside the radial channels

Channel number	$\dot{Q}$ x10^{-4} / m^3 s^{-1}	%$^{(*)}$
1	1.58	10
2	2.81	17
3	1.13	7
4	1.03	6
5	1.01	6
6	1.09	7
7	1.27	8
8	1.57	10
9	2.05	13
10	2.63	16

$^{(*)}\% = Q_{radial\ channel} / Q_{inlet}$; Q_{inlet} = 1.23 x10^{-3} m^3 s^{-1}

The temperature distribution of the fluid (oil) and of the solid domain (discs) can be found in Figure 12a and Figure 12b, respectively.

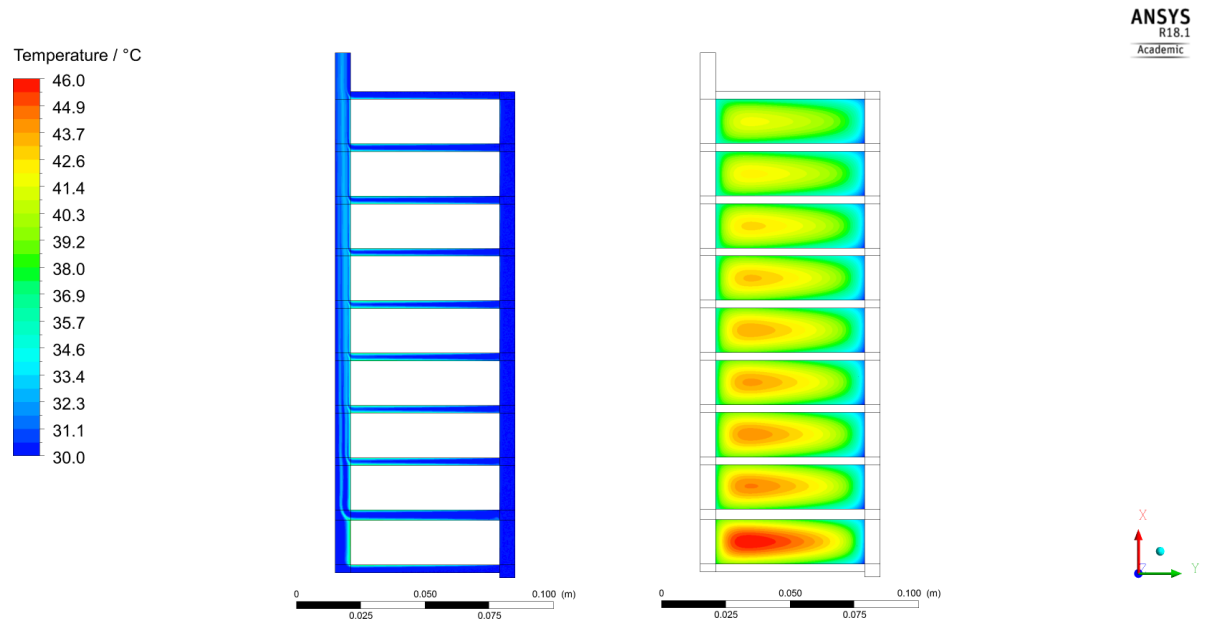

a) b)

Figure 12 - Temperature distribution in the pass (Figure 9a) a) fluid domain; b) solid domain

Figure 12 shows that the fluid enters the pass with 30 °C and exits the pass win a mass weighted average temperature of 31.5 °C. The average increase of oil temperature in the considered first pass is 1.5 °C. The outlet maximum temperature determined was 32.3 °C. While it may seem a small increase, one must remember that there's five more passes in this winding, plus the low-tension winding, multiplying both windings by 3, which is the number of phases. Looking at the outlet temperature as maximum temperature values in a winding pass

may lead into mistakes, because as it will be shown below, the temperatures inside the pass are higher than the ones at the outlet.

The variation of the average oil temperature across both axial (internal and external) and radial channels is illustrated in Figure 13.

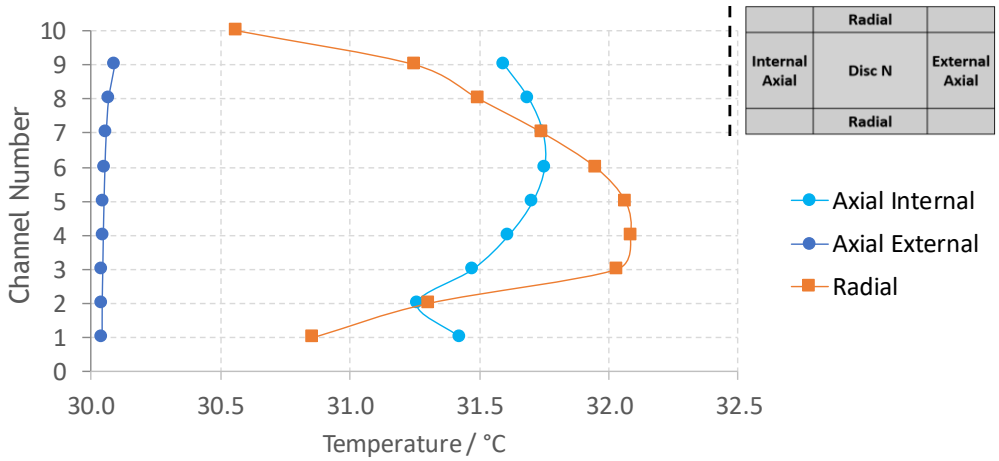

Figure 13 - Average oil temperature along the axial (internal and external) and radial channels of the 9 discs

The results in Figure 13 demonstrate that the oil temperature slightly changes in the axial external region of the 9 discs (varying less than 0.1 °C). As the oil flows from the external region to the inner parts of the pass (i.e. through radial and internal axial channels, Figure 13) the temperature rises (e.g. from 30.1 °C in the axial external region to 32.1 °C in the fourth radial channel). The temperature in the radial channels varies between 30.6 and 32.1 °C. The temperature is lower in the radial channels that have higher flow rates (channels 1,2,8,9 and 10, Table 9). In the axial internal region, the temperature varies between 31.3 and 31.8 °C.

The average disc wall temperatures in the four surfaces of each disc (i.e. internal and external axial surface, top and bottom radial surface) are shown in Figure 14.

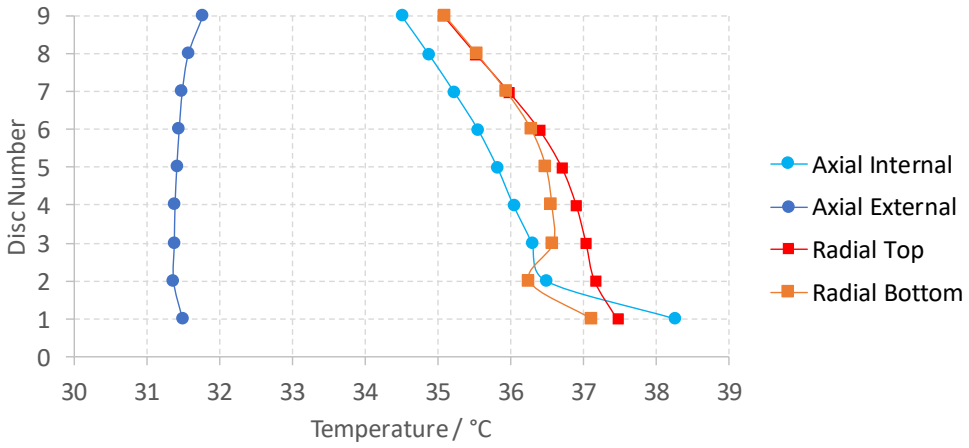

Figure 14 - Average disc wall temperature along the axial (internal and external) and radial (top and bottom) walls of the 9 discs

Figure 14 shows that for each disc, the temperature of the radial top wall is higher than the bottom wall. This difference between these temperatures decrease with the height of the pass, the maximum difference being 0.9 °C on the second disc and 0 °C in disc 9. In the axial internal region, the temperature is higher in the lower parts of the pass (e.g. 38.3 °C in disc 1), as there is less oil flowing close to the walls (Table 9). The axial external part varies less than 0.5 °C. The highest temperature gradient occurs in the axial internal region, varying between 34.5 and 38.3 °C.

The average disc surface temperature (i.e. area weighted average of the temperature of the four disc walls) is shown in Figure 15.

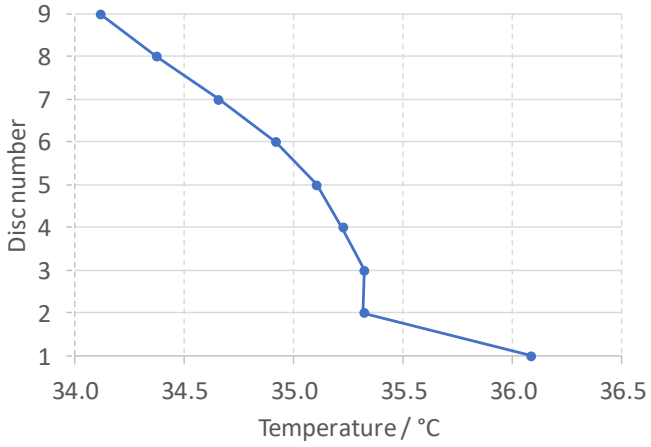

Figure 15 - Average disc surface temperature of the 9 discs

As it is previously noticed in Figure 12b, the discs at the bottom of the pass have the highest temperature and the consecutive discs have a gradual decrease in temperature. Therefore, the average temperature of the surface decreases along the pass (Figure 15), starting at 36.1 °C in disc 1 and ending at 34.1 °C in disc 9. The disc with the coldest and

hottest average surface temperature is disc number 9 and 1, respectively. The hot spot temperature on the pass was also determined, as it will be important for water content in paper calculations. The value obtained is 39.6 °C and is located in radial top wall of disc 1 (Figure 17a).

The following analyzes of water content in paper (WCP) considers three chosen values of water content in oil at the inlet (WCO, section 0). Four different temperatures (i.e. the temperature of the hot spot, of the total disc surface, of each wall of the disc and discrete values obtained in the disc walls) were considered to understand the deviations of assuming average or discrete values of temperature on the water distribution inside the pass. The first temperature evaluated is the average disc surface, which can be seen in Figure 16.

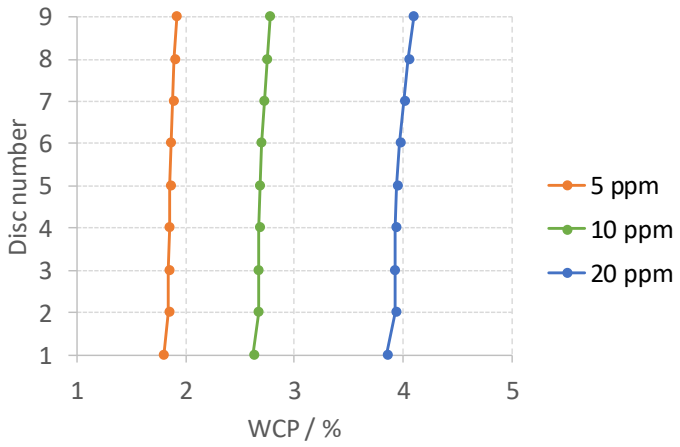

Figure 16 - Water content in paper (WCP) of each disc obtained considering the average surface temperature of the disc

Figure 16 shows that the WCP calculated using the average disc surface temperature are 1.86, 2.74 and 4.05 % for a WCO of 5, 10 and 20 ppm, respectively. As expected, these WCP values are slightly higher than the values obtained considering the hot spot temperature (39.6 °C). The WCP for the hot spot temperature are 1.59, 2.41 and 3.51 % for a WCO of 5, 10 and 20 ppm, respectively.

To have the distribution of WCP in the disc walls, the wall temperature profiles of the discs should be evaluated. The discs chosen for this analysis were the first one and the last in the pass (Disc number 1 and 9, Figure 9), as they have the highest and lowest temperature, respectively. The temperature profiles and the corresponding WCP profiles for each disc, regarding the three different WCO at the inlet, can be found in Figure 17. The length in axial walls (blue series,Figure 17) increases with the disc height and the length in radial walls (red and orange series, Figure 17) increases from the interior part of the winding to the exterior. The WCP obtained using the hot spot temperature was also shown (dashed line, Figure 17).

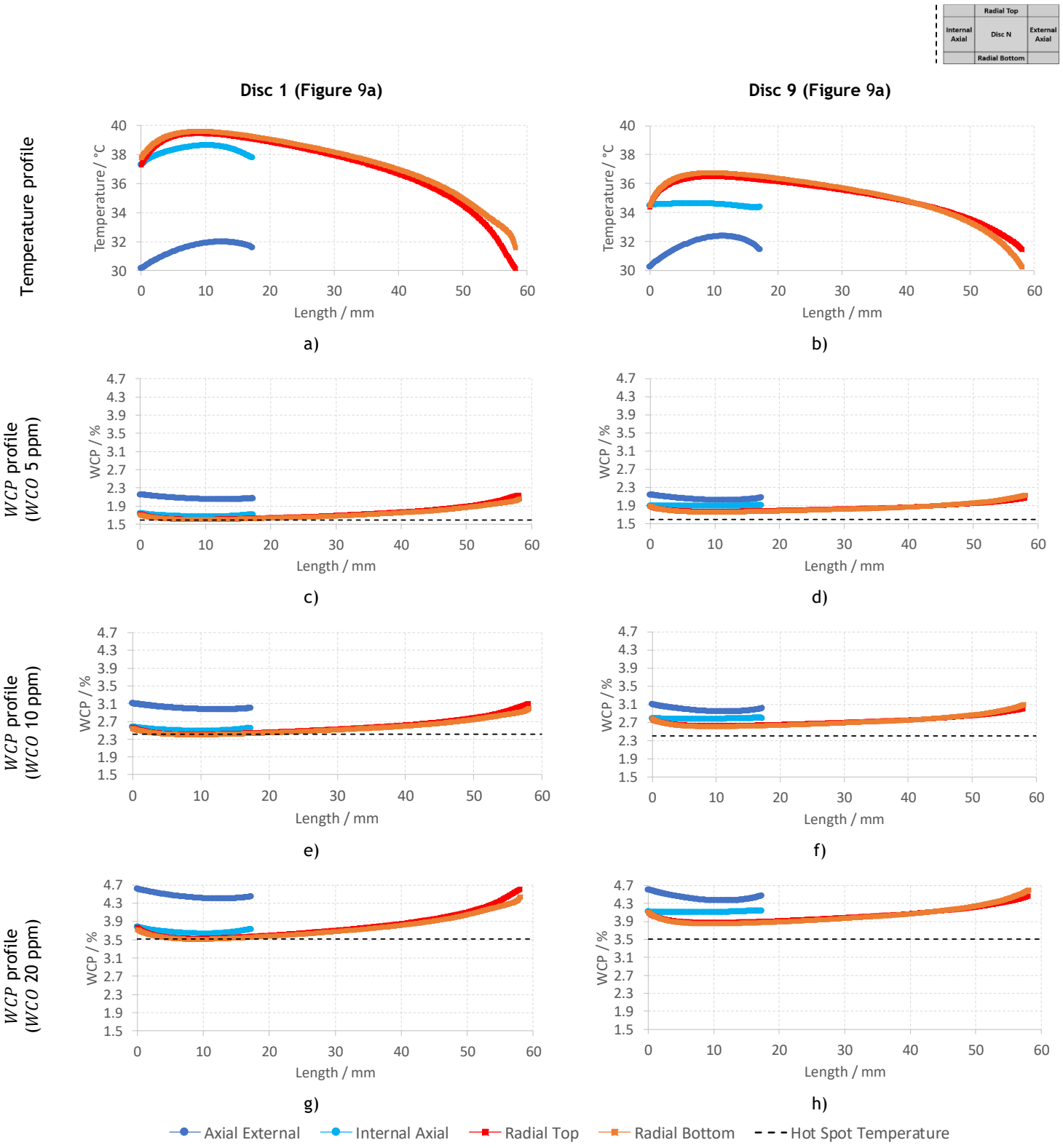

Figure 17 - Temperature (a and b) and WCP profiles (c, d, e, f, g and h) obtained for the discs with the highest and lowest surface temperature (disc 1 and 9, respectively); The paper water content was calculated assuming different temperatures (each surface of the disc and the hot spot value), for three values of inlet water content in oil (WCO): 5, 10 and 20 ppm

In the two discs studied (disc 1 and 9) the walls with the highest gradient of temperature are the radial walls (Figure 17a and b). Along the length of both radial walls the temperature increases until a maximum value located nearby 10 mm and after that position the temperature significantly decreases (more than 4 °C, Figure 17a and b). For example, for disc 1(Figure 17a) the maximum temperature is 39.6 °C and the deviation between the maximum and minimum temperature is 8.0 and 9.3 °C, respectively for the bottom and top walls. For disc 9, the maximum temperature is 36.7 °C and the deviation between the maximum and minimum temperature is 5.1 and 6.5 °C, respectively for the top and bottom walls. The maximum temperature variance is 8 °C in the bottom wall and 9.3 °C in the top wall of the first disc; 6.5 °C in the bottom wall and 5 °C in the top wall of disc 9. Both axial walls have an increase and decrease of temperature in an "inverted u" shape, as it can be seen in Figure 17a and b. The maximum variance of temperature on the axial external wall is 1.8 °C for disc 1 and 2.1 °C for disc 9. As for the axial internal wall, the maximum variance is 1.3 °C for disc 1 and 0.3 °C for disc 9. The axial external wall has the lowest temperature value out of the four walls (30.2 °C for both discs, Figure 17a and b), making it the zone where the water content is higher.

As for the WCP (Figure 17c to h), in both discs the axial external wall (dark blue series) has higher values of WCP than the axial internal wall (light blue series). However, when comparing the water predictions in the radial walls, the two discs show curves of WCP with different tendency. For example, for disc 1 (Figure 17c, e and g) the radial top wall (red series) has slightly higher values of WCP than the radial bottom wall. This doesn't happen in disc 9, because when comparing the temperature profiles of the radial walls of the two discs (1 and 9, Figure 17a and b) there is a slight difference in the behavior of the profiles approximately after the 30 mm.

For a value of 5 ppm of WCO, in disc 1 (Figure 17c) the internal axial wall has about 0.4 % less WCP than the axial external wall (the internal axial wall varies between 1.65 and 1.73 %, while the axial external wall varies between 2.03 to 2.14 %). Both axial walls have somewhat the same WCP variance of 0.10 %. The radial walls have approximately the same WCP distribution, starting at 1.60 % and ending at 2.10 %. Comparing the estimation calculated using the hot spot temperature, the maximum deviation is 0.55 % WCP. As for disc 9, this deviation has the same value but the gradients of WCP in the walls are smaller (0.38 %, Figure 17d). The maximum value of WCP is 2.14 % and is found in the axial external wall and in the radial bottom wall. The minimum value of WCP is 1.8 % and is found in the radial walls. Therefore, using the hot spot temperature estimation induces at least a 0.2 % WCP error in disc 9.

When the WCO increases, the WCP distribution gets more heterogeneous. For 10 ppm (Figure 17f) the maximum deviation of WCP (between the maximum WCP value obtained through the wall WCP profiles and the WCP estimated using the hot spot temperature) is

0.69 % WCP (3.10 and 2.41 %, respectively) while for 20 ppm is 1.10 % (4.61 and 3.51 %, respectively). The zone with most water accumulated in disc 1 is in the top of the internal axial wall. For disc 9, the zone changes to bottom of the external axial wall.

Finally, a comparison of the WCP value obtained using the four different approaches was done to disc 9 with a WCO of 20 ppm. Firstly, using the hot spot temperature (39.6 °C), the value estimated is 3.51 %. Using the average surface disc surface temperature (34.1 °C), the value estimated is 4.15 %. Using the average wall temperature of the axial external wall (chosen out of the four disc walls of disc 9 as it has the highest WCP value, 31.8 °C) the value estimated is 4.48 %. Using the maximum value of WCP in the same wall, the value obtained is 4.60 %.

4.2 Distribution of paper water content inside a winding

The results of the four simulations described in 3.3.2 are presented below. The velocity magnitude profiles of simulations 1 and 2 (inlet velocity equal to 0.10 and 0.20 m s^{-1}, respectively) are shown in Figure 18.

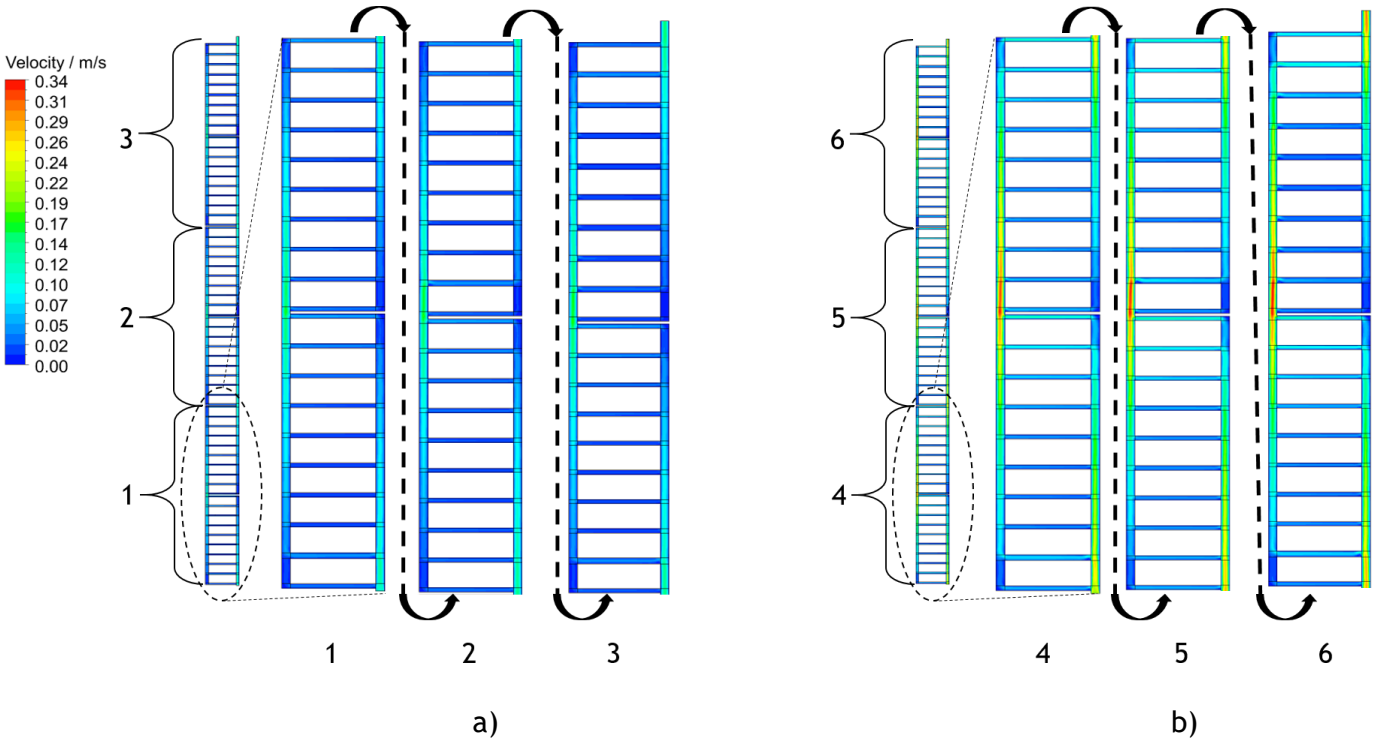

Figure 18 - Velocity magnitude distribution inside a winding with 54 discs (Figure 7a): a) simulation 1 (inlet velocity 0.10 m s^{-1}) b) simulation 2 (inlet velocity 0.20 m s^{-1})

The oil enters the winding at the bottom (1 in Figure 18a, 4 in Figure 18b) with an uniform velocity (0.10 and 0.20 m s^{-1} in Figure 18a and b, respectively), travels through the winding (from 1 to 3 in Figure 18a, from 4 to 6 in Figure 18b) and exits with an area weighted average velocity of 0.10 and 0.20 m s^{-1}, as expected. The temperature distribution of the fluid (oil) and of the solid domain (discs) can be found in Figure 19, for simulations 1 to 4.

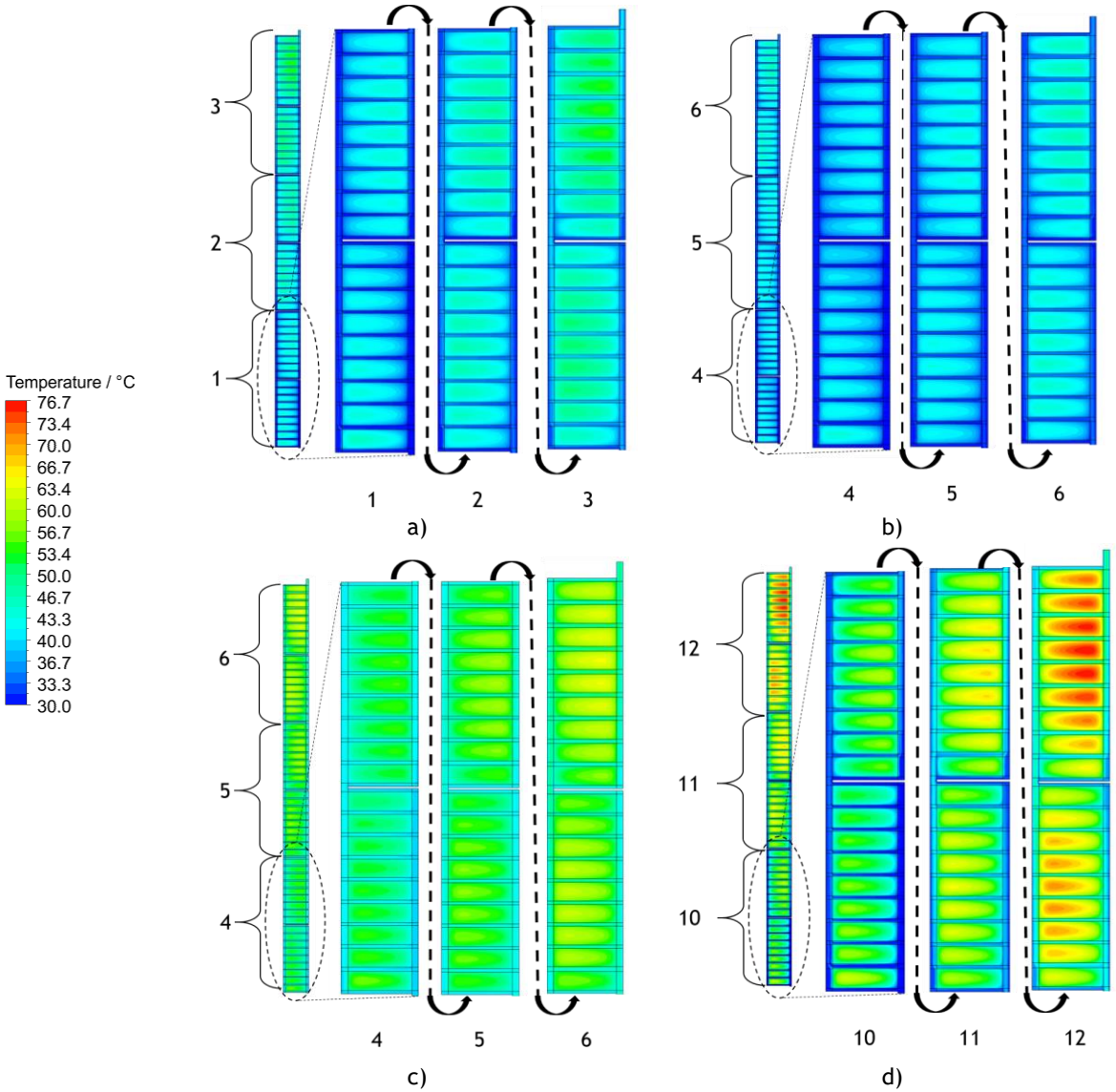

Figure 19 - Temperature distribution in the winding a) simulation 1 b) simulation 2 c) simulation 3 d) simulation 4 ; conditions from Table 7

Figure 19 shows that the fluid enters the winding with 30 °C in simulations 1, 2 and 4. The temperature at the inlet and outlet of the winding for simulations 1 to 4 can be found in Table 10.

Table 10 -Oil temperature (average and maximum) obtained in the inlet and outlet of the winding

	Mass Weighted Average Temperature / °C			Outlet Maximum Temperature / °C
	Inlet	Outlet	Δ	
Simulation 1	30.0	38.5	8.5	41.1
Simulation 2	30.0	34.3	4.3	35.8
Simulation 3	40.0	48.5	8.5	50.8
Simulation 4	30.0	46.9	16.9	51.2

From the results shown in Table 10 we can conclude that for a higher velocity (simulation 2) the average outlet temperature is lower (34.3 °C) when compared with a lower velocity (simulation 1, 38.5 °C), because the fluid flows faster through the winding, which decreases the amount of heat transferred to the fluid. Increasing the temperature at the inlet (simulation 3) doesn't change the variation of temperature the fluid undergoes (i.e. the average temperature difference in the inlet and outlet is 8.5 °C for simulation 1 and 3). Doubling the heat sources in the discs (simulation 4) causes the highest temperature out of the four simulations (51.2 °C) and the highest variation in temperature (between 30 °C and 51.2. °C).

A comparison of average disc surface temperature can be found in Figure 20.

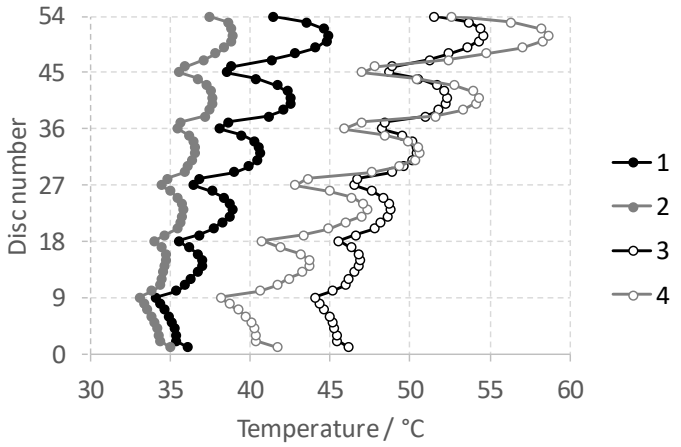

Figure 20 - Effect of the winding operation conditions (of inlet temperature and velocity and of discs heat source) on the average disc surface temperature (simulation 1 to 4, Table 7)

The simulation 2 of Figure 20 that has the lowest variation of the average disc surface temperature, where the lowest temperature is 33 °C and the highest temperature is 39 °C. The highest variation occurs in simulation 4, varying between 38 to 59 °C. A higher variation in the

average surface temperature values (as seen in simulation 4, Figure 20) will result in a higher range of WCP values.

To check if the average disc surface temperature profiles in simulations 1 (30 °C at the inlet) and 3(40 °C at the inlet) were the same but with a deviation of 10 °C, both temperature profiles along the winding were compared, subtracting 10 °C to the results obtained in simulation 3. The comparison is shown in Figure 21.

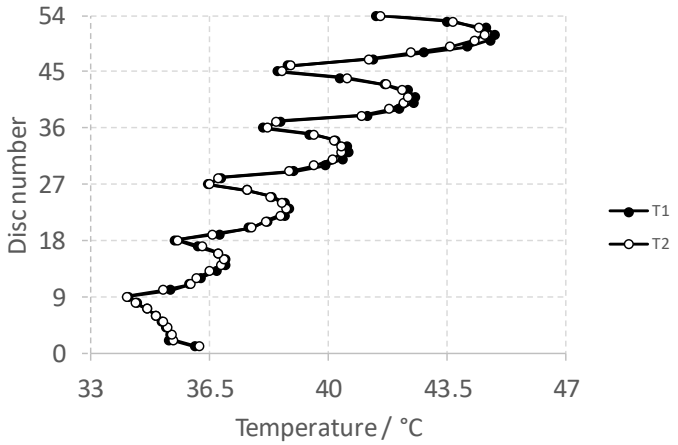

Figure 21 – Comparison of average disc surface temperature of T_1 and T_2

As shown in Figure 21, both profiles have similar results, where the maximum absolute deviation is 0.2 °C. This deviation is higher on the hotter discs of each pass, and more evident in the upper half of the winding. This means that for a value T_3 between T_1 and T_2 the results obtained for the average disc surface temperature will be approximately equal to the ones obtained in T_1 adding $T_3 - T_1$ to T_1 results.

The area weighted average temperature surface of each disc and the respective WCP in the discs for each simulation can be found in Figure 22.

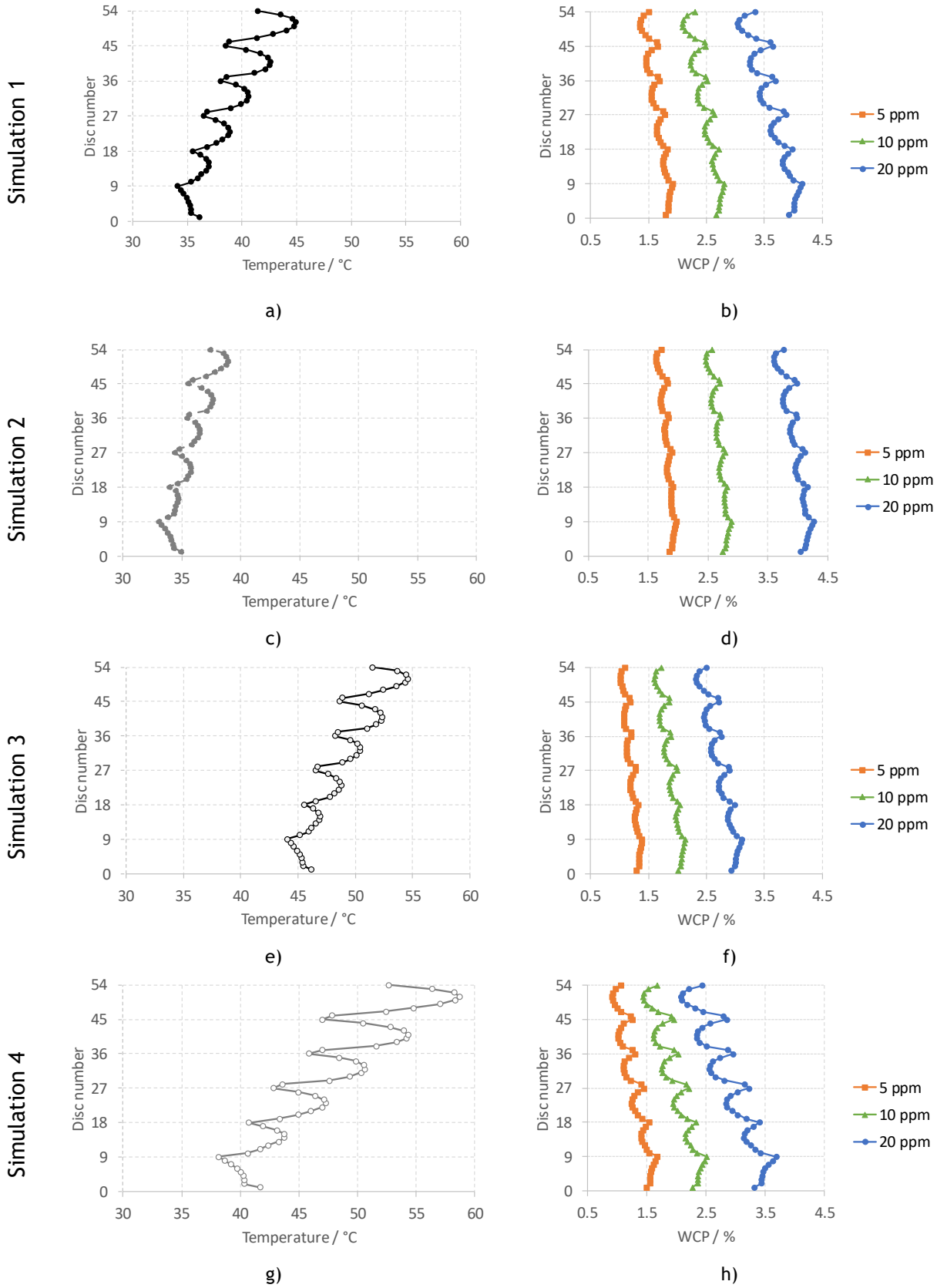

Figure 22 - Area weighted average disc surface temperatures (a, c, e and g) and WCP profiles (b, d, f and h) obtained for the 54 discs of the winding; The paper water content was calculated assuming the average disc surface temperature for three values of inlet water content in oil (WCO): 5, 10 and 20 ppm (simulation 1 to 4, Table 7)

In all simulations shown in Figure 22 disc 9 has the lowest average disc surface temperature (34.1, 33.1, 44.1, 38.2 °C for simulations 1, 2, 3 and 4, respectively) while disc 51 has the highest average disc surface temperature (44.9, 38.9, 54.6, 58.7 °C for simulations 1, 2, 3 and 4, respectively, as seen in Figure 22a , c, e, g). As expected, the opposite tendency is obtained for the WCP predictions (Figure 22b, d, f, h). The values of WCP in simulation 2 are higher than in the other simulations for the three WCO analysed, since the temperature values are the lowest of the four simulations. The highest variation of WCP in a singular WCO analysis (highest gradient of WCP values) was obtained in simulation 4 for a WCO of 20 ppm (Figure 22h), varying from 2.08 % to 3.68 %. The lowest variation of WCP in a singular WCO analysis was obtained in simulation 2 for a WCO of 5 ppm (Figure 22d), varying from 1.63 % to 1.97 %.

The maximum and minimum temperatures at the disc walls were determined for each simulation and it was found that the results were independent of the conditions applied. The maximum temperature was found on disc number 51 in the radial bottom wall. As for the minimum temperature, it was found on disc number 2 in the external axial wall. However, the difference of temperature in the axial external wall of the disc 2 and 9 is 0.029 °C, which means that the temperature values can be considered equal. As disc 9 has the lowest average disc surface temperature, discs 9 and 51 were chosen for a more in-depth analysis of the wall temperature distribution.

The hot spot for each simulation (maximum temperature out of every disc surface, for every simulation this was found on disc 51) was determined and WCP was calculated for the different WCO at the inlet. The results can be found in Table 11.

Table 11 – Hot spot temperature obtained for each simulation for three values of inlet water content in oil (WCO): 5, 10 and 20 ppm (simulation 1 to 4, Table 7)

Simulation	1	2	3	4
Hot spot temperature / °C	49.1	42.4	58.8	66.9
WCP for WCO 5 ppm / %	1.16	1.46	0.92	0.72
WCP for WCO 10 ppm / %	1.83	2.23	1.43	1.12
WCP for WCO 20 ppm / %	2.67	3.26	2.07	1.61

The conclusions obtained from the results on Table 10 are similar to the ones from Table 11. By increasing the disc losses (simulation 4), the highest temperature out of the four simulations is reached (66.9 °C). Increasing 10 °C at the inlet (simulation 3) makes the hot spot temperature increase by 9.7 °C (58.8 °C for simulation 3 compared with 49.1 °C for simulation 1). By having a higher velocity (simulation 2), the fluid that reaches the higher parts of the winding has less temperature (42.4 °C), resulting in a lower temperature at the walls.

Values of WCP obtained varied between 0.72 and 3.26 %. As expected, the values of WCP increase then the WCO increases as well.

The area weighted average wall temperatures were obtained for discs 9 and 51 and the WCP was compared with the ones from Table 11. The results and the deviation from the values calculated using the hot spot temperature can be seen in Table 12, Table 13 and Table 14 for the WCO of 5, 10 and 15 ppm, respectively. The values in bold represent the maximum and minimum deviations in relation to the WCP calculated using the hot spot temperature (Table 11).

Table 12 – Average WCP profiles obtained for the discs with the highest and lowest surface temperature (disc 9 and 51, respectively); The paper water content was calculated assuming different temperatures of the disc wall for a WCO of 5 ppm

	Simulation 1				**Simulation 2**				**Simulation 3**				**Simulation 4**			
	Disc 9		**Disc 51**		**Disc 9**		**Disc 51**		**Disc 9**		**Disc 51**		**Disc 9**		**Disc 51**	
Wall	WCP / %	Δ	WCP / %	Δ	WCP / %	Δ	WCP / %	Δ	WCP / %	Δ	WCP / %	Δ	WCP / %	Δ	WCP / %	Δ
Axial External	2.05	0.89	1.34	0.18	2.08	0.62	1.62	0.16	1.49	0.57	1.01	0.09	1.94	**1.22**	0.91	0.19
Axial Internal	1.89	0.73	1.53	0.37	1.96	0.50	1.83	0.37	1.37	0.45	1.11	0.19	1.63	0.91	1.11	0.39
Radial Bottom	1.85	0.69	1.27	0.11	1.93	0.47	1.55	0.09	1.35	0.43	0.97	**0.05**	1.56	0.84	0.83	0.11
Radial Top	1.86	0.70	1.26	0.10	1.93	0.47	1.55	0.09	1.35	0.43	0.97	**0.05**	1.57	0.85	0.83	0.11

Table 13 - Average WCP profiles obtained for the discs with the highest and lowest surface temperature (disc 9 and 51, respectively); The paper water content was calculated assuming different temperatures of the disc wall for a WCO of 10 ppm

	Simulation 1				**Simulation 2**				**Simulation 3**				**Simulation 4**			
	Disc 9		**Disc 51**		**Disc 9**		**Disc 51**		**Disc 9**		**Disc 51**		**Disc 9**		**Disc 51**	
Wall	WCP / %	Δ	WCP / %	Δ	WCP / %	Δ	WCP / %	Δ	WCP / %	Δ	WCP / %	Δ	WCP / %	Δ	WCP / %	Δ
Axial External	2.98	1.15	2.07	0.24	3.02	0.79	2.44	0.21	2.28	0.85	1.58	0.15	2.85	**1.73**	1.41	0.29
Axial Internal	2.78	0.95	2.33	0.50	2.87	0.49	2.71	0.48	2.11	0.68	1.77	0.34	2.46	1.34	1.75	0.63
Radial Bottom	2.74	0.91	1.97	0.14	2.83	0.60	2.35	0.12	2.08	0.65	1.52	**0.09**	2.37	1.25	1.29	0.17
Radial Top	2.74	0.91	1.97	0.14	2.83	0.60	2.35	0.12	2.08	0.65	1.52	**0.09**	2.37	1.25	1.29	0.17

Table 14 - Average WCP profiles obtained for the discs with the highest and lowest surface temperature (disc 9 and 51, respectively); The paper water content was calculated assuming different temperatures of the disc wall for a WCO of 20 ppm

	Simulation 1				Simulation 2				Simulation 3				Simulation 4			
	Disc 9		Disc 51		Disc 9		Disc 51		Disc 9		Disc 51		Disc 9		Disc 51	
Wall	WCP / %	Δ	WCP / %	Δ	WCP / %	Δ	WCP / %	Δ	WCP / %	Δ	WCP / %	Δ	WCP / %	Δ	WCP / %	Δ
Axial External	4.42	1.80	3.02	0.35	4.48	1.22	3.56	0.30	3.32	1.25	2.30	0.23	4.22	**2.61**	2.05	0.44
Axial Internal	4.10	1.43	3.40	0.73	4.24	0.98	3.99	0.73	3.08	1.01	2.57	0.50	3.60	1.99	2.55	0.94
Radial Bottom	4.04	1.37	2.88	0.21	4.18	0.92	3.43	0.17	3.03	0.96	2.21	**0.14**	3.46	1.85	1.87	0.26
Radial Top	4.04	1.37	2.87	0.20	4.19	0.93	3.43	0.17	3.03	0.96	2.21	**0.14**	3.46	1.85	1.86	0.25

In Table 12, Table 13 and Table 14, the maximum value of WCP is in the axial external wall of disc 9, using the variables of simulation 2. The minimum value of WCP is in the radial walls of disc 51, using the variables of simulation 3. As for the deviations, these are highest in the axial external wall of disc 9 in simulation 4, and lowest in the radial walls of disc 51 in simulation 3. The maximum deviation between both methods is 2.61 % WCP, 1.61 % when calculated the hot spot temperature and 4.22 % with the average wall temperature. The amount of water present using the average wall temperature is more than the double estimated using the hot spot temperature.

The temperature profiles and the corresponding WCP profiles were obtained for discs 2 and 51, regarding the three different WCO values at the inlet. The WCP obtained using the hot spot temperature was also presented to compare the results with this estimation. The figures presented are the ones in which the results are more relevant to the analysis pretended. The remaining results are shown in Appendix 4.

Disc 51 has the maximum temperature gradient occurring in simulation 4 and the maximum WCP gradient occurs in the same simulation and is shown in Figure 23a and b, respectively.

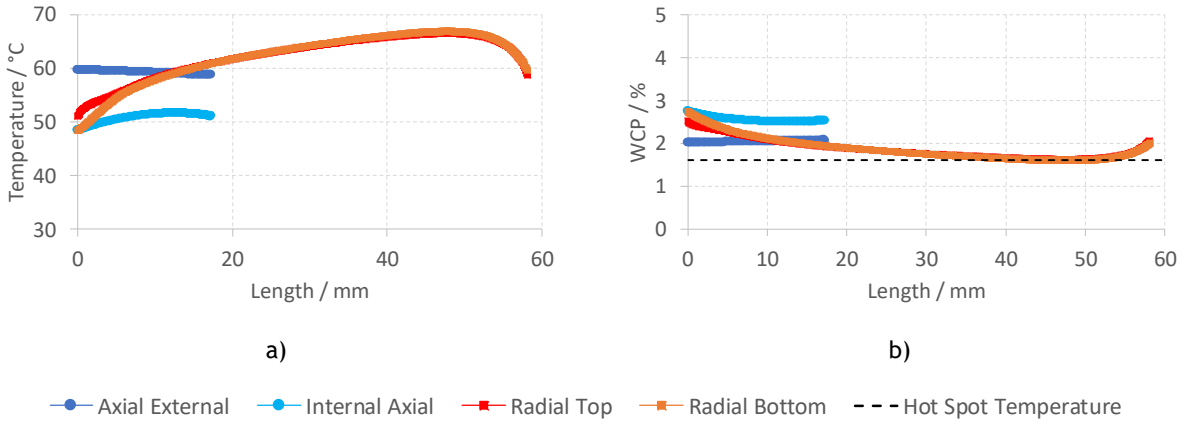

Figure 23 - Temperature (a) and WCP profiles (b) obtained along the walls of disc 51; The paper water content was calculated assuming different temperatures and an inlet WCO of 20 ppm (simulation 4, Table 6)

The radial bottom wall (orange series) has a temperature gradient of 18.5 °C (from 48.3 to 66.9 °C, Figure 23a) and a WCP gradient of 1.14 % (1.61 to 2.74 %, Figure 23b). The maximum value of WCP in the walls is 2.74 % (in the axial internal wall and the radial bottom wall, represented in light blue and orange, respectively) and the maximum temperature reached is 66.9 °C (radial bottom wall). The maximum deviation of the WCP value compared to the hot spot temperature estimated WCP is also shown in Figure 23b. The WCP on both the axial internal wall and the radial bottom wall (2.74 %) can be 1.13 % higher than the value estimated using the hot spot temperature (1.61 %).

In disc 9, the maximum temperature gradient also occurs in simulation 4, as shown in Figure 24a. The maximum WCP gradient occurs in the same simulation and is shown in Figure 24b.

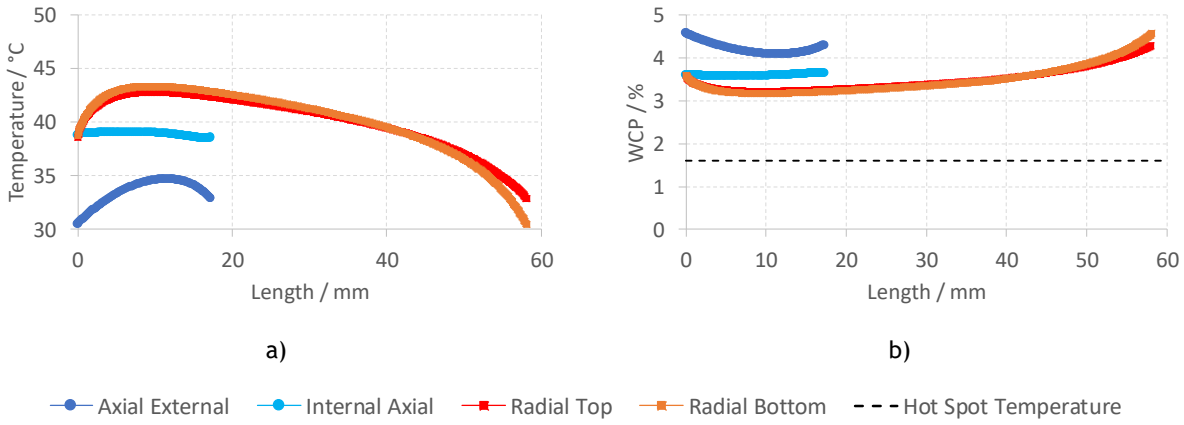

Figure 24 - Temperature (a) and WCP profiles (b) obtained along the walls of disc 9; The paper water content was calculated assuming different temperatures and an inlet WCO of 20 ppm (simulation 4, Table 6)

The radial bottom wall has a temperature gradient of 12.9 °C (30.5 to 43.4 °C, Figure 24a) and a WCP gradient of 1.40 % (3.18 to 4.58 %, Figure 24b). The maximum value of WCP in the walls is 4.57 % (on the axial external wall and radial bottom wall) and the maximum

temperature reached is 43.4 °C (radial bottom wall). The maximum deviation of the WCP value compared to the hot spot temperature estimated WCP is also shown in Figure 24b. The WCP on both the axial external wall and the radial bottom wall (4.57 %) can be 2.99 % higher than the value estimated using the hot spot temperature (1.61 %).

5 Conclusions

In this work the thermal and water content in paper (WCP) profiles were obtained in a power transformer winding using numerical simulations. Different approaches for WCP calculations using temperature values were considered and compared.

The first analysis was made to the first pass of the winding. The flow distribution on the radial channels was heterogeneous, having preference (higher flow rate) on the bottom and top channels of each pass (radial channels 1, 2, 8, 9 and 10). The temperature profile was obtained, and the hot spot temperature was calculated (e.g. 39.6 °C, on the radial top wall of disc 1). The discs with the highest and lowest temperature were discs 1 and 9, respectively. The WCP predictions along the winding discs showed a heterogeneous distribution along the discs surfaces, where the higher values of WCP are obtained in the external regions of the discs. For example, in disc 1, for a value of 5 ppm of WCO, the external axial wall has about 0.4 % more WCP than the internal wall. This tendency increases with the augment of WCO. For the same disc (1) and a higher WCO value (e.g. 20 ppm), the difference between the WCP external and internal wall is 0.78 % WCP.

The results also indicated that predictions of water content in paper considering the hot spot temperature may be misleading since the values can be less than half of the maximum value determined on critical conditions. For example, in disc 9, the WCP values obtained for a WCO of 20 ppm using the hot spot temperature was 3.51 %, while the WCP predictions based on disc 9 average surface temperature, disc 9 average wall temperature and disc 9 minimum wall temperature (as disc 9 will have the highest WCP values) resulted in higher values of WCP such as 4.15, 4.42 and 4.60 %, respectively.

A parametric analysis was then made considering the whole winding. The inlet velocity, inlet temperature and disc heat sources were tested. The main results were:

1) The higher the disc heat sources (simulation 4), the higher the gradients of temperature, which consequently implies higher WCP gradients inside the winding;
2) For a higher inlet velocity, the temperature and WCP gradients will be lower;
3) The discs with the highest and lowest temperature do not change between simulations (i.e. remained the same in the four simulations) and they were discs 51 and 9, respectively. The obtained hot spot temperature was 49.1, 42.4, 58.8 and 66.9 °C respectively for simulations 1, 2, 3 and 4.

At the critical scenario (WCO of 20 ppm, simulation 4), the maximum deviation between WCP using the hot spot temperature (1.61 %) and the calculated maximum WCP value was 2.61

% WCP (4.57 %, on the axial external wall of disc 9). This indicates that the prediction using the hot spot temperature may lead into underestimated values of WCP.

The approach described in this thesis allowed the prediction of the water content in paper distributed inside a winding. The results were obtained in steady-state. However, in future works the transient behaviour of water migration inside the paper/winding should be considered, which implies a more detailed approach (i.e. more phenomena). This increases the complexity of the system of equations that need to be solved. As a suggestion to reduce the computational resources needed for the mathematical model, a model of reduced order should be used (e.g. THNM). In this situation if the discs geometry is simplified (e.g. by considering an average temperature instead the distribution along the discs surface) the results showed in this thesis highlight some relevant deviations in WCP (i.e. deviations in maximum value).

Efacec has a proprietary model of reduced order that considers the heat transfer and fluid motion (i.e. THNM). However, it neglects the water presence. The approach proposed in this thesis can be integrated in the aforementioned model to predict the WCP.

6 Assessment of the work done

6.1 Objectives Achieved

The water distribution inside a power transformer winding was successfully obtained. The effect of the inlet velocity, inlet temperature and of disc heat sources on WCP predictions was studied.

6.2 Future Work

For future work it is suggested testing more scenarios that probably will have a significant effect on WCP predictions such as a heterogeneous distribution of the heat in the discs along the radial symmetry or geometrical parameters such as the vertical divisions. Experimental data should be obtained under controlled conditions applied to the PT to compare with the numerical simulations.

To improve the accuracy of the proposed approach in this thesis, instead of the generic equilibrium curves of WCP, specific curves should be obtained for the particular materials used in Efacec's PTs.

The implementation of the WCP calculation on THNMs could give a general overview on the WCP values inside the winding with quick time-to-solution.

Once enough knowledge is extracted from steady-state simulations, the logical next step would be the implementation of the transient regime. For that, some variables need to be determined such as the sorption and desorption rates, the heat source variation through time, and the ambient temperature difference during the day-night cycle and during different seasons (these vary with the geographical location where the PT will be placed).

Another line of research with great interest is the study of the paper. The implementation of ageing equations with the results obtained from simulations can give a better prediction on the PT's lifespan. Using this information coupled with simulations changes can be done to the PT to extend its lifetime.

6.3 Final Assessment

The results obtained from this work are just the tip of the iceberg. There is still a lot of research that needs to be done on the phenomena occurring inside a power transformer and how they affect its lifespan. That being said, it is important to start with a simplified study to gain a basis to be able to support more complex cases.

In my opinion this work made me learn a lot of things. Besides introducing me to the industry sector, it made me understand what researching in a company is like and how everyday a new problem arises that needs a solution. I also developed my working method, my organizational skills and ability to present results. I am thankful for the opportunity and hope that this work is useful in any way possible.

References

[1] J. H. Harlow, *Electric Power Transformer Engineering*. CRC Press, 2004.

[2] E. Hajidavalloo and M. Mohamadianfard, "Effect of sun radiation on the thermal behavior of distribution transformer," *Appl. Therm. Eng.*, vol. 30, no. 10, pp. 1133–1139, 2010.

[3] S. Zervos, "Natural and accelerated ageing of cellulose and paper: A literature review," in *Cellulose: Structure and Properties, Derivatives and Industrial Uses*, no. April, 2010, pp. 155–203.

[4] U. U. B. M. Ali, "Transformer Life Prediction Using Data From Units Removed From Service," 2013.

[5] S. Teszenszky, "History of Transformers," *IEEE Power Eng. Rev.*, vol. 16, no. 12, p. 9, 1996.

[6] S. R. and S. N. M. Whelan, "History of Transformers," 2014. [Online]. Available: http://www.edisontechcenter.org/Transformers.html. [Accessed: 03-May-2018].

[7] G. Hollings, "How transformers work," 2013. [Online]. Available: https://www.abb-conversations.com/2013/09/how-transformers-work/. [Accessed: 03-May-2018].

[8] Hydroelectric Research and Technical Services Group, "Transformers : Basics, Maintenance and Diagnostics," *Transform. diagnostics*, vol. 1, no. April, p. 256, 2005.

[9] J. F. Mora, *Máquinas eléctricas*. McGraw-Hill Interamericana de España S.L., 2008.

[10] O. Joel, "Parts of a Power Transformer," 2018. [Online]. Available: https://owlcation.com/stem/Parts-of-a-power-transformer. [Accessed: 14-May-2018].

[11] M. J. Heathcote and D. P. Franklin, "The J & P Transformer Book: A Practical Technology of the Power Transformer," *J P Transform. B.*, 2012.

[12] Electrical Services Group, "Why Is Copper Used So Much In Making Electrical Wires?," 2018. [Online]. Available: http://www.esg-ct.com/New-Haven-Electrical/electrical/copper-making-electrical-wires/. [Accessed: 14-May-2018].

[13] G. K. Frimpong, T. V. Oommen, and R. Asano, "A survey of aging characteristics of cellulose insulation in natural ester and mineral oil," *IEEE Electr. Insul. Mag.*, vol. 27, no. 5, pp. 36–48, 2011.

[14] NEUROtiker, "Cellulose molecular structure," 2007. [Online]. Available: https://upload.wikimedia.org/wikipedia/commons/0/07/Cellulose_Sessel.svg. [Accessed: 25-Jun-2018].

[15] A. I. for Conservation of Historic and A. Works, *Preprints of Papers Presented at the Fifteenth Annual Meeting: Vancouver, British Columbia, Canada, May 20-24, 1987*. The Institute, 1987.

[16] R. D. Medina, A. A. Romero, E. E. Mombello, and G. Rattá, "Assessing degradation of power transformer solid insulation considering thermal stress and moisture variation," *Electr. Power Syst. Res.*, vol. 151, pp. 1–11, 2017.

[17] L. E. Lundgaard, W. Hansen, D. Linhjell, and T. J. Painter, "Aging of Oil-Impregnated Paper in Power Transformers," *IEEE Trans. Power Deliv.*, vol. 19, no. 1, pp. 230–239, 2004.

[18] A. M. Emsley, R. J. Heywood, M. Ali, and X. Xiao, "Degradation of cellulosic insulation in power transformers .4. Effects of ageing on the tensile strength of paper," *Sci. Meas. Technol. IEE Proc. -*, vol. 147, no. 6, pp. 285–290, 2000.

[19] CIGRE Working Group A2.18, "Life management techniques for power transformer," *Tech. Broch. CIGRE*, no. 227, 2003.

[20] B. García, J. C. Burgos, Á. M. Alonso, and J. Sanz, "A moisture-in-oil model for power transformer monitoring - Part I: Theoretical foundation," *IEEE Trans. Power Deliv.*, vol. 20, no. 2 II, pp. 1417–1422, 2005.

[21] T. K. Saha and P. Purkait, *Transformer Ageing: Monitoring and Estimation Techniques*. Wiley, 2017.

[22] Y. Du, M. Zahn, B. C. Lesieutre, A. V Mamishev, and S. R. Lindgren, "Moisture equilibrium in transformer paper-oil systems," *IEEE Electr. Insul. Mag.*, vol. 15, no. 1, pp. 11–20, 1999.

[23] SpinningSpark, "Transformer winding formats," 2012. [Online]. Available: https://upload.wikimedia.org/wikipedia/commons/f/fe/Transformer_winding_formats.jpg. [Accessed: 12-Jun-2018].

[24] P. S. Georgilakis, "Spotlight on modern transformer design," *Power Systems*, vol. 38. 2009.

[25] R. A. Robert M. Del Vecchio, Bertrand Poulin, Pierre T. Feghali, Dilipkumar M. Shah, *Transformer Design Principles With Applications*. 2017.

[26] T. K. P. P. Saha, *Transformer Ageing*. 2017.

[27] A. S. Tyuftyaev, M. K. Gadzhiev, M. A. Sargsyan, P. L. Akimov, and N. A. Demirov, "The effect of gas bubbles on electrical breakdown in transformer oil," *J. Phys. Conf. Ser.*, vol. 774, no. 1, pp. 0–6, 2016.

[28] F. M. Clark, "Factors Affecting the Mechanical Deterioration of Cellulose Insulation," *Trans. Am. Inst. Electr. Eng.*, vol. 61, no. 10, pp. 742–749, 1942.

[29] B. Sparling and J. Aubin, "Assessing Water Content in Insulating Paper of Power Transformers," no. Figure 1, 2007.

[30] L. J. Zhou, G. N. Wu, and J. Liu, "Modeling of transient moisture equilibrium in oil-paper insulation," *IEEE Trans. Dielectr. Electr. Insul.*, vol. 15, no. 3, pp. 872–878, 2008.

[31] M. Mukherjee, D. Martin, S. V. Kulkami, and T. Saha, "A mathematical model to measure instantaneous moisture content in transformer insulation cellulose," *IEEE Trans. Dielectr. Electr. Insul.*, vol. 24, no. 5, pp. 3207–3216, 2017.

[32] CIGRE Working Group A2.30, "Moisture Equilibrium and Moisture Migration within Transformer Insulation Systems," *Tech. Broch. CIGRE*, no. 349, 2008.

[33] N. Pan and P. Gibson, *Thermal and moisture transport in fibrous materials*, First ed. Wookhead Publishing Limited, 2006.

[34] P. Przybylek, “The influence of cellulose insulation aging degree on its water sorption properties and bubble evolution,” *IEEE Trans. Dielectr. Electr. Insul.*, vol. 17, no. 3, pp. 906–912, 2010.
[35] V. Sarfi, S. Mohajeryami, and A. Majzoobi, “Estimation of water content in a power transformer using moisture dynamic measurement of its oil,” *High Volt.*, vol. 2, no. 1, pp. 11–16, 2017.
[36] H. Lomax, T. H. Pulliam, and D. W. Zingg, “Fundamentals of Computational Fluid Dynamics,” 2001.
[37] H. M. Campelo *et al.*, “Detailed CFD analysis of ODAF power transformer,” *Int. Colloq. Transform. Res. Asset Manag.*, no. May 2014, pp. 1–10, 2009.
[38] S. Khandan and S. Tenbohlen, “CFD Study of Fluid Flow and Temperature Distributions in a Power Transformer Winding,” no. Icdl, pp. 29–32, 2017.
[39] F. Torriano, M. Chaaban, and P. Picher, “Numerical study of parameters affecting the temperature distribution in a disc-type transformer winding,” *Appl. Therm. Eng.*, vol. 30, no. 14–15, pp. 2034–2044, 2010.
[40] M. Quintela, H. Campelo, E. Energia, and P. Labbé, “Assumptions and Numerical Parameters Influencing the Accuracy of Thermal Models for Core-Type Power Transformer,” vol. 00, no. August, 2017.
[41] H. M. R. Campelo, M. A. Quintela, F. Torriano, P. Labbe, and P. Picher, “Numerical thermofluid analysis of a power transformer disc-type winding,” *34th Electr. Insul. Conf. EIC 2016*, pp. 362–365, 2016.
[42] J. Zhang and X. Li, “Oil Cooling for Disk-Type Transformer Windings—Part 1: Theory and Model Development,” *IEEE Trans. Power Deliv.*, vol. 21, no. 3, pp. 1318–1325, 2006.
[43] K. Kurita, M. Hirano, and K. Hiraishi, “Static electrification and partial discharges caused by oil flow in forced oil cooled core type transformers,” *IEEE Trans. Power Appar. Syst.*, vol. PAS-98, no. 4, pp. 1259–1267, 1979.
[44] ANSYS, *ANSYS Fluent Theory Guide*, vol. 15317, no. November. 2013.
[45] Nynas, “Nytro Taurus Standard Grade,” 2017.
[46] P. P. K. N. W. Normalizacyjnych, *Insulating Liquids - Oil-impregnated Paper and Pressboard - Determination of Water by Automatic Coulometric Karl Fischer Titration (IEC 60814:1997)*. Polski Komitet Normalizacyjny, 2002.
[47] I. Power and E. Society, *IEEE Guide for Acceptance and Maintenance of Insulating Mineral Oil in Electrical Equipment*, no. June. 2015.
[48] Y. A. Çengel, *Heat and Mass Transfer - A pratical approach*, Third edit. McGraw-Hill Science/Engineering/Math, 2007.
[49] B. R. Munson, A. P. Rothmayer, and T. H. Okiishi, *Fundamentals of Fluid Mechanics, 7th Edition*. Wiley, 2012.

Appendix 1 – Mesh independence tests

Mesh independence study were performed to understand how refined the mesh should be. The ideal mesh has the least computing time needed without compromising the results.

1.1 Geometry 1

Table 15 includes the selected meshes for comparison.

Table 15 – Meshes used for the mesh independence study of geometry 1 (Figure 25a)

Mesh Number	Number of y Divisions	Number of x Divisions	Number of Elements
1	20	581	11 620
2	20*	581	11 620
3	20	1 162	23 240
4	50	581	29 050
5	100	581	58 100
6	200	581	116 200

*-No bias

In most cases a bias was introduced in the y division, to better represent the phenomena occurring near the walls. No bias was used in the x division.

Four different lines were drawn at different lengths of the domain to evaluate the progression of the velocity profile. Another line was drawn perpendicularly to the others and across the whole length to determine the max velocity and calculate the entry region length. Figure 25a represents the geometry with the lines drawn. Figure 25b shows the lengths chosen.

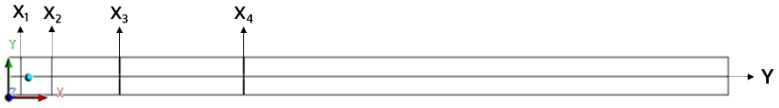

a)

Line	Dimensions / mm
X1	1
X2	3.5
X3	9
X4	19
Y	22

b)

Figure 25 - a) geometry chosen and lines used for analysis; b) lengths at each line was drawn

The entry region length is the length a flow needs to fully develop. With the conditions used for this test (as shown in Table 19 and Table 20) and the line Y, the velocity magnitude was determined across the length. The velocity increases until it reaches its maximum value. This point is called the entry region length and can be found in Figure 26.

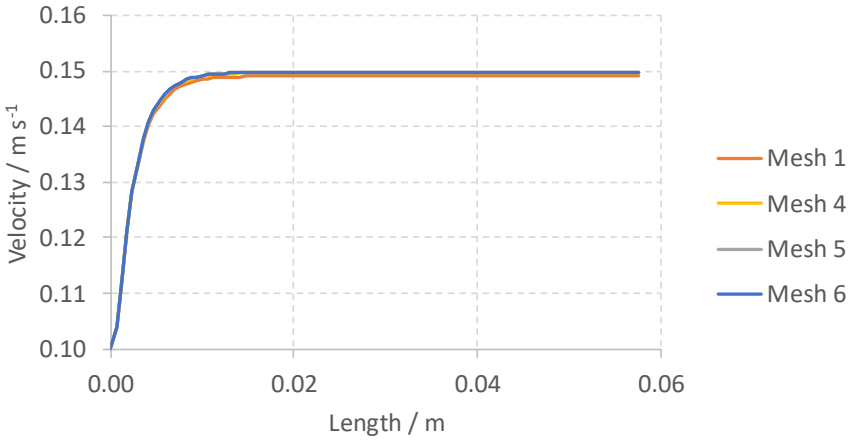

(a)

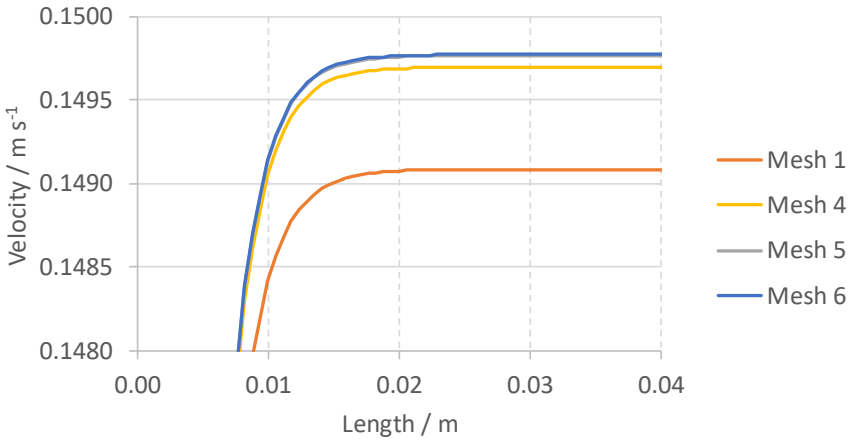

(b)

Figure 26 - Velocity magnitude at line Y. (a)Whole domain; (b) Zoomed in for detail

The entry region length is determined to be at approximately 0.018 m. The flow is fully developed by the line X4, so the velocity profile at this line should resemble a Poiseuille flow's behaviour, given by Equation 16. As it can be seen in Figure 26b, Mesh 1 and 4 velocity magnitude is lower than the ones in mesh 5 and 6. As mesh 5 the same results as mesh 6 while having fewer elements, it should be the mesh chosen. However more tests were performed to solidify this choice.

A comparison was made between mesh 1 and mesh 2 to find out if the bias had any influence in the velocity profile. The analysis can be found in Figure 27. Figure 27a shows the velocity profile at line X4 of mesh 1, while Figure 27b shows the velocity profiles at line X4 in mesh 2. A comparison of both is made in Figure 27c.

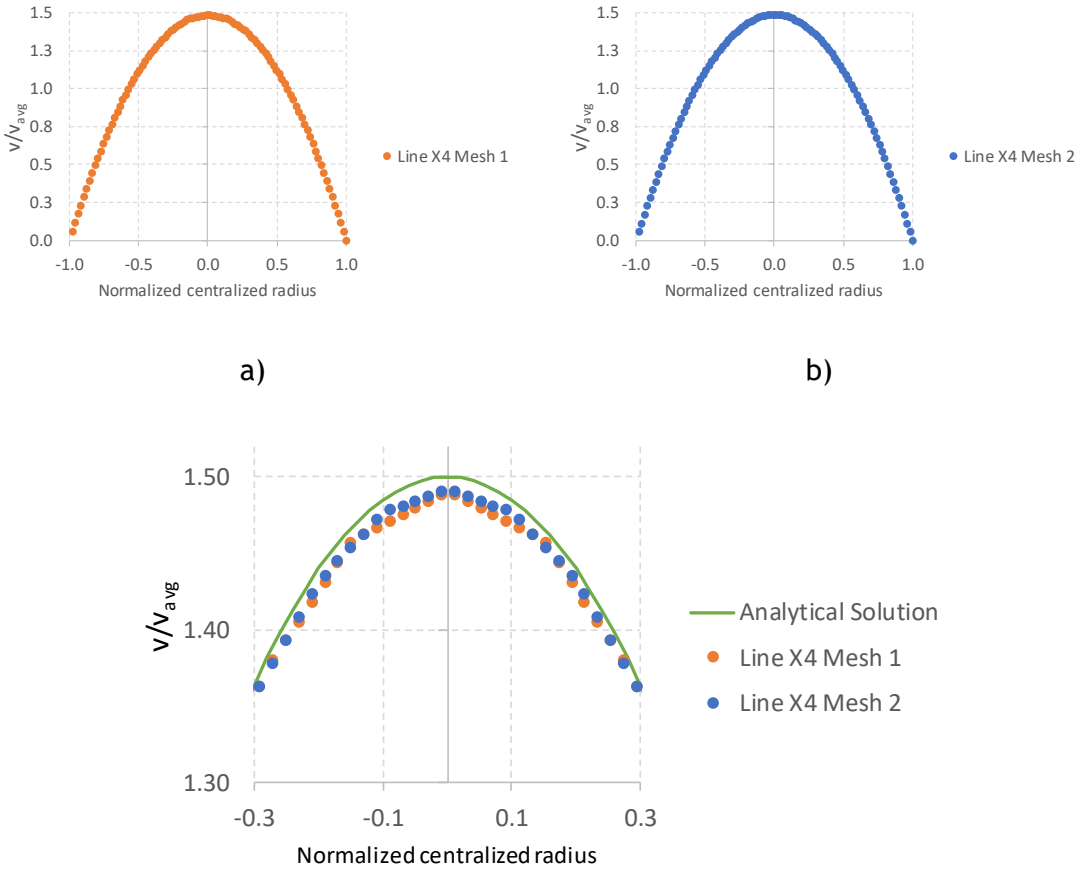

Figure 27 - a) Mesh 1 velocity profiles; b) No bias velocity profiles; c) Comparison of a) and b)

The difference verified in Figure 27c is due to the different element sizes that the bias causes. It is safe to consider that there is no significant difference between both meshes. As bias will be an important factor in upcoming studies regarding heat and mass transfer, the unbiased mesh was disregarded.

The next test was made between meshes 1 and 3 to check if the number of x divisions had any impact in the flow development. Figure 28 shows the velocity profiles at lines X1 and X4 and compares line X4 with the analytical solution of a fully developed flow.

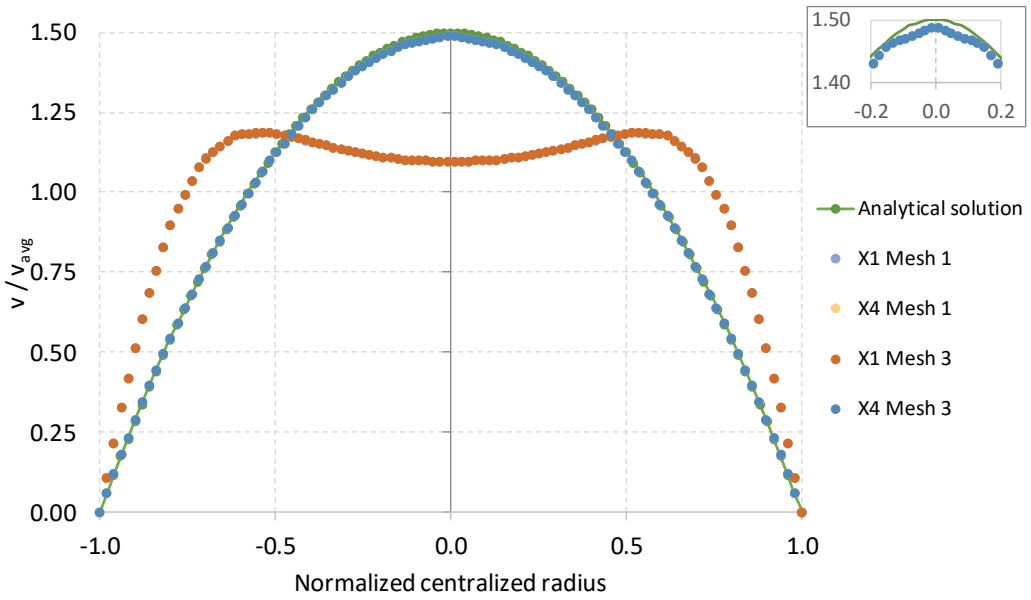

Figure 28 - Comparison between meshes 1 and 3

The number of x divisions between mesh 1 and 3 does not have any impact on the velocity profiles, therefore mesh 3 was discarded, as it has more elements than needed.

The final comparison was made with meshes 1, 4, 5 and 6. The velocity profiles at line X4 were obtained and compared with the analytical solution. This can be found in Figure 29.

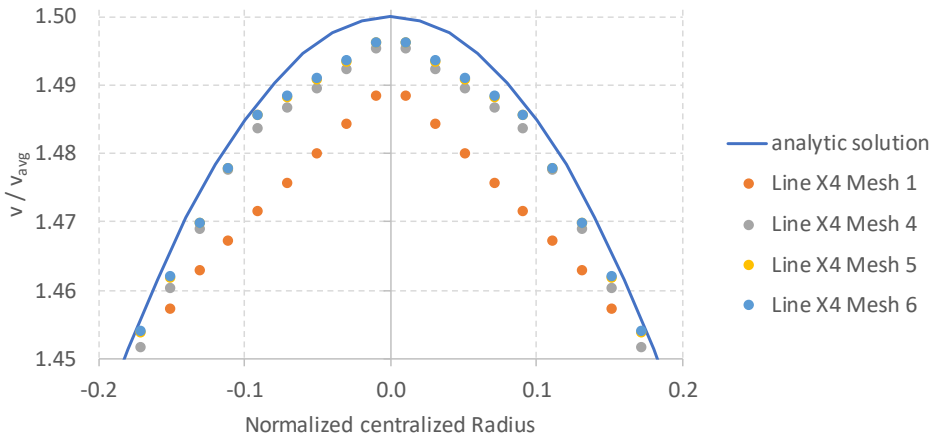

Figure 29 - Velocity profiles at line X4 for meshes 1, 4, 5 and 6 and comparison with the analytical solution

Mesh 1 has the biggest deviation from the analytical solution. Meshes 5 and 6 are almost completely overlapped and are the ones that better represent the fully developed flow. As such, mesh 5 was the one chosen to proceed with the verification of the transfer model.

1.2 Geometry 2

Table 16 includes the selected meshes for comparison.

Table 16 – Meshes used for the mesh independence study of geometry 2 (Figure 9a)

Mesh Number	First Element Size / mm	Number of Elements
7	0.5	41 166
8	0.1	435 662
9	0.05	986 232
10	0.1	3 580 010

The velocity profiles were obtained at 5 different regions of the pass and were compared to check if the results obtained were independent of the mesh or not. The regions chosen are shown in red in Figure 30.

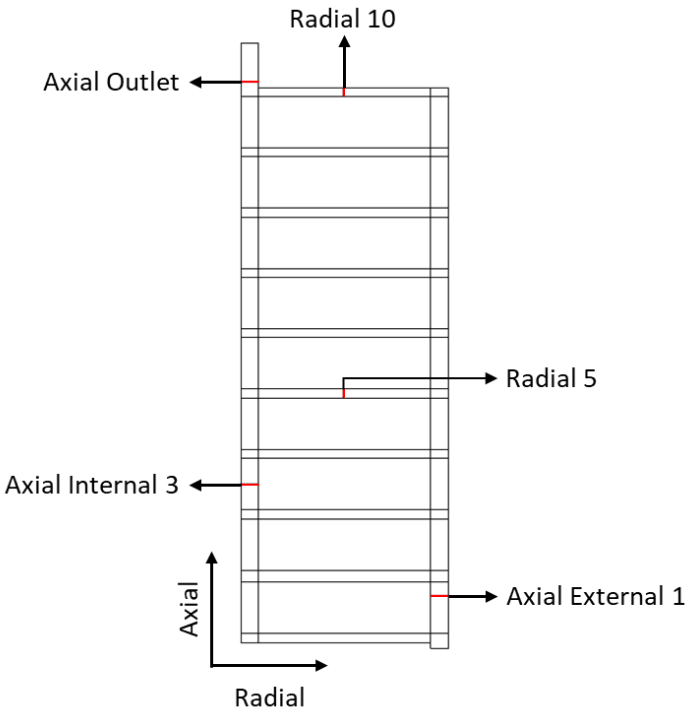

Figure 30 - Lines chosen for the study of mesh independence using geometry 2 (Figure 9a)

The velocity profiles at the axial external 1 line are shown in Figure 31.

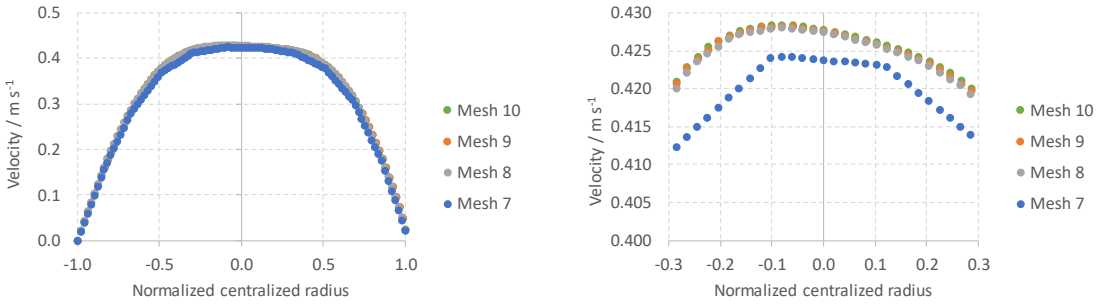

Figure 31 - Velocity profiles at axial external 1 (Figure 30)

The velocity profiles at the axial internal 3 line are shown in Figure 32.

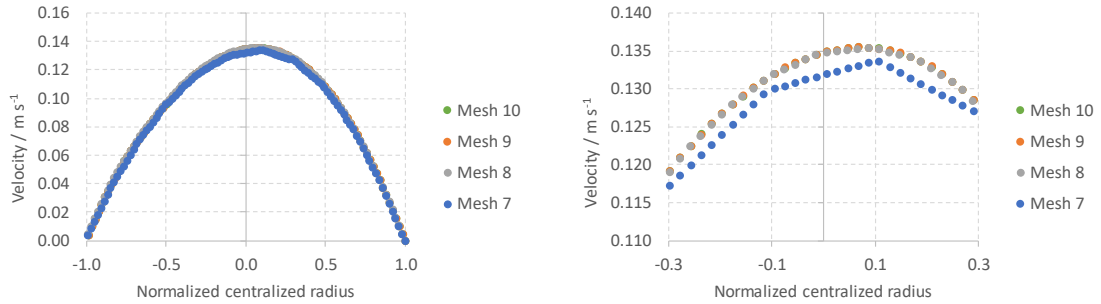

Figure 32 - Velocity profiles at axial internal 3 (Figure 30)

The velocity profiles at the axial outlet line are shown in Figure 33.

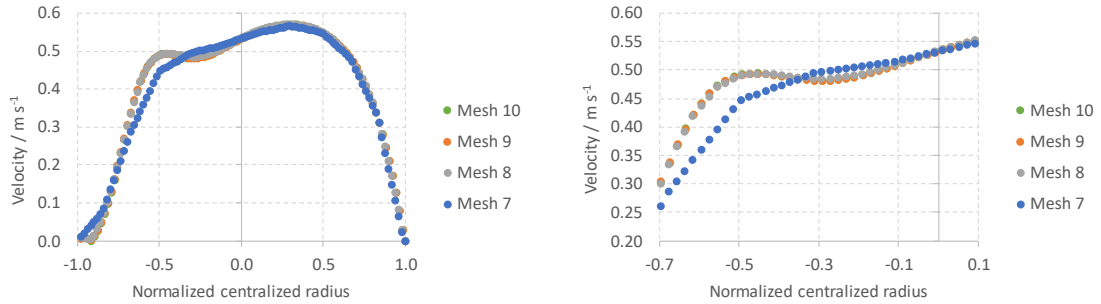

Figure 33 - Velocity profiles at axial outlet (Figure 30)

The velocity profiles at the radial 5 line are shown in Figure 34.

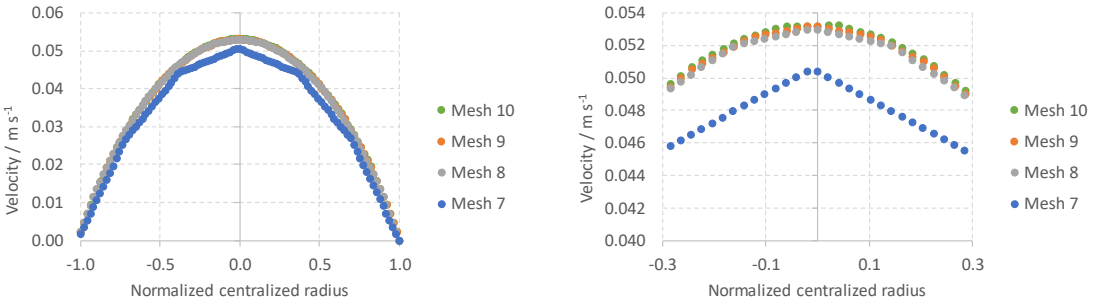

Figure 34 - Velocity profiles at radial 5 (Figure 30)

The velocity profiles at the radial 10 line are shown in Figure 35.

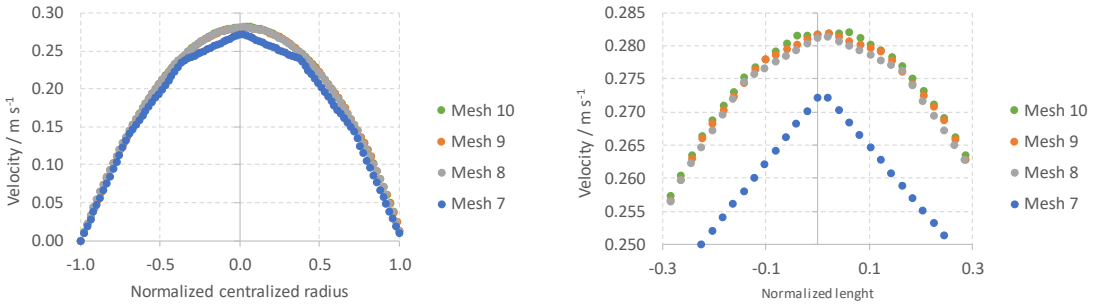

Figure 35 - Velocity profiles at radial 10 (Figure 30)

Every mesh displays close results except for mesh 7. Mesh 8 was chosen, as it has the best results with less resources needed.

1.3 Geometry 3

As the basis of geometry 2 and 3 are the same, a mesh with the same properties was chosen for the winding calculations. The number of elements is displayed in Table 17.

Table 17 - Details of the mesh used for winding simulations

Mesh Number	First Element Size / mm	Number of Elements
11	0.1	2 607 414

The mesh obtained is shown in Figure 36.

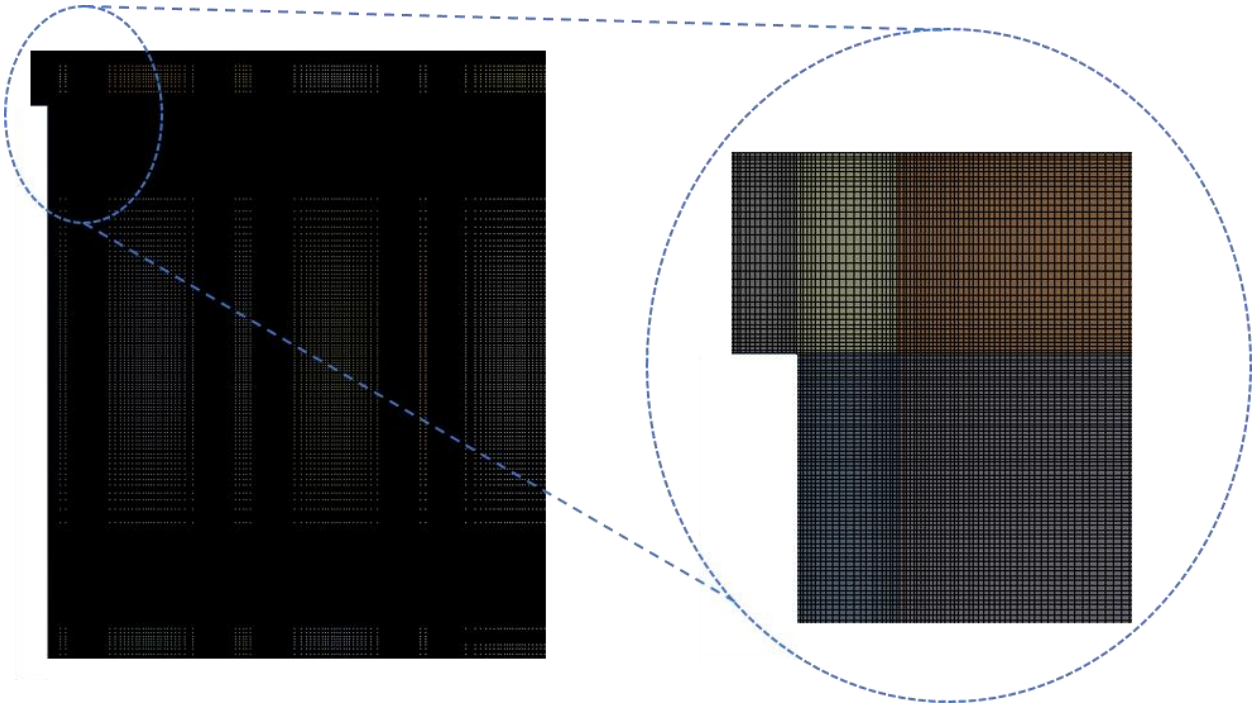

Figure 36 – Mesh used in the simulations

Appendix 2 - Equivalent thermal conductivity calculation

To further simplify the simulation, instead of representing the paper and copper that are present in the winding, an equivalent material was considered. The equivalent thermal conductivity was then determined to proceed with the simulations.

As it can be seen by Figure 10a, the material has different radial and axial conformations and therefore both radial and axial thermal conductivities must be calculated.

As the geometry adopted is axisymmetric, the radial resistance for a single component can be calculated with the following equation: [48]

$$R_{Radial} = \frac{ln\left(\frac{R_{ext}}{R_{int}}\right)}{2\pi Lk} \tag{8}$$

where R_{ext} is the outer radius of the part, R_{int} is the inner radius, L is the height and k is the thermal conductivity of the material.

The axial resistance for a single component can be calculated with the following equation: [48]

$$R_{Axial} = \frac{L}{k * A} \tag{9}$$

where A can be calculated by equation 2.

The thermal conductivities of paper and copper can be found in Table 18.

Table 18 - Thermal conductivities of copper and paper

k_{copper}	388.50 W m^{-1} °C^{-1}
$k_{Kraft\ Paper}$	0.16 W m^{-1} °C^{-1}

The values of the disc dimensions needed for calculations can be found in Figure 10b. The thermal resistance is a sum of resistances such as the ones in Figure 37.

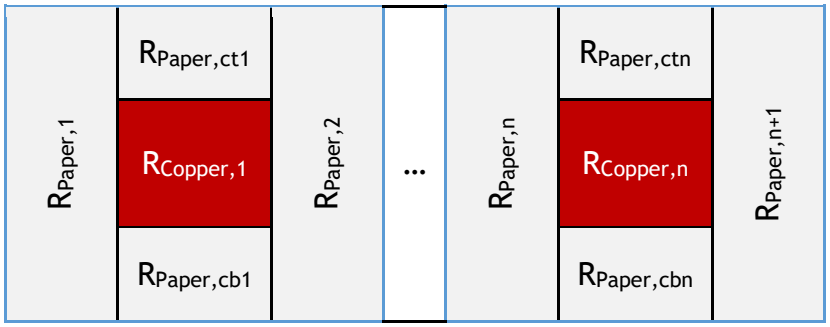

Figure 37 – Thermal resistances in a disc

Each segment surrounded by blue repeats itself throughout the disc. There are 18 repeated parts in a disc. However, as the radius increases, the value of the resistance varies.

The radial equivalent resistance can be calculated by equation 10.

$$R_{eq}^{Radial} = \sum_{i=1}^{n+1} R_{paper,i} + \sum_{i=1}^{n} R_{eq,i} \tag{10}$$

where n is the number of repeated parts. $R_{eq,i}$ can be calculated by equation 11.

$$\frac{1}{R_{eq,n}} = \frac{1}{R_{Paper,ctn}} + \frac{1}{R_{Copper,n}} + \frac{1}{R_{Paper,cbn}} \tag{11}$$

where $R_{Paper,ctn}$ is the resistance of the paper above the copper at the n part and $R_{Paper,cbn}$ is the resistance of the paper below the copper at the n part. In fact, $R_{Paper,ctn}$ and $R_{Paper,cbn}$ have the same value. Equation 11 can then be rewritten as equation 12.

$$R_{eq,n} = \frac{2}{R_{Paper,cn}} + \frac{1}{R_{Copper,n}} \tag{12}$$

Once R_{eq}^{Radial} is calculated then k_{eq}^{Radial} can be determined by equation 13.

$$k_{eq}^{Radial} = \frac{\ln\left(\frac{R_{ext}}{R_{int}}\right)}{2\pi L R_{eq}^{Radial}} \tag{13}$$

The value of k_{eq}^{Radial} calculated is 0.37 W m^{-1} °C^{-1}.

As for the axial axis, the thermal resistance can be calculated with equation 14.

$$\frac{1}{R_{eq}^{Axial}} = \sum_{i=1}^{n+1} \frac{1}{R_{paper,i}} + \sum_{i=1}^{n} \frac{1}{R_{eq,i}} \tag{14}$$

$R_{eq,i}$ is calculated with equation 11. Once R_{eq}^{Axial} is calculated than k_{eq}^{Axial} can be determined by equation 15.

$$k_{eq}^{Axial} = \frac{L_{disc}}{R_{eq}^{Axial} A_{disc}} \tag{15}$$

The value of k_{eq}^{Axial} calculated is 1.18 W m^{-1} °C^{-1}.

Appendix 3- Verification of the transfer model accuracy

3.1 Model assumptions and equations

To have a better understanding on how the solver is working and since there is no empirical data to compare the simulated results with, a simpler case was made to check whether the results given by the solver make sense or not. For that, a simplified geometry with known analytical solution was chosen to make this analysis.

3.1.1 Geometry

Figure 38 displays the geometry used for this test. The dimensions used are the ones of a radial channel on the pass, so the results are closer to reality. The geometry was created using ANSYS® SpaceClaim.

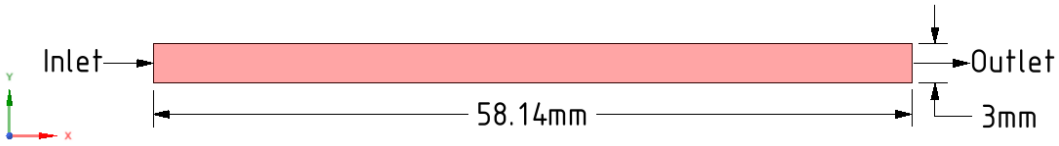

Figure 38 - Geometry chosen for solver validation

Further mesh independence tests were made and can be found in Appendix 1. The mesh chosen was Mesh 5.

3.1.2 Flow Validation

The first validation test was made to verify whether the simulated results accurately represent the analytical solution or not. Since the geometry is a 2D rectangular duct, the results could be compared to the analytical solution of a fully developed velocity profile, given by

$$v = v_{max}\left(1 - \left(\frac{r^2}{R^2}\right)\right) \tag{16}$$

where v is the velocity at a radius r, v_{max} is the maximum velocity and R is the duct radius. For a 2D rectangular duct, v_{max} is equal to 1.5 times the average velocity, $\bar{v}$. [49]

The boundary conditions applied are shown in Table 19.

Table 19 - Boundary Conditions

Boundary Type	Boundary Condition	U_0 / m s^{-1}	P_0
Inlet	Velocity	0.1	-
Outlet	Pressure	-	0
Walls	No Slip	-	-

The oil properties applied to the fluid are described in Table 20.

Table 20 - Properties of oil at 60 °C

Properties	Oil
Density ρ kg^{-1} m^{-3}	846
Specific Heat cp / kJ kg^{-1} °C^{-1}	2005
Thermal Conductivity k / kJ kg^{-1} °C^{-1}	0.130
Dynamic Viscosity μ / Pa s	0.005

The comparison between the analytical solution and the developed velocity profile obtained through simulation can be found in Figure 39.

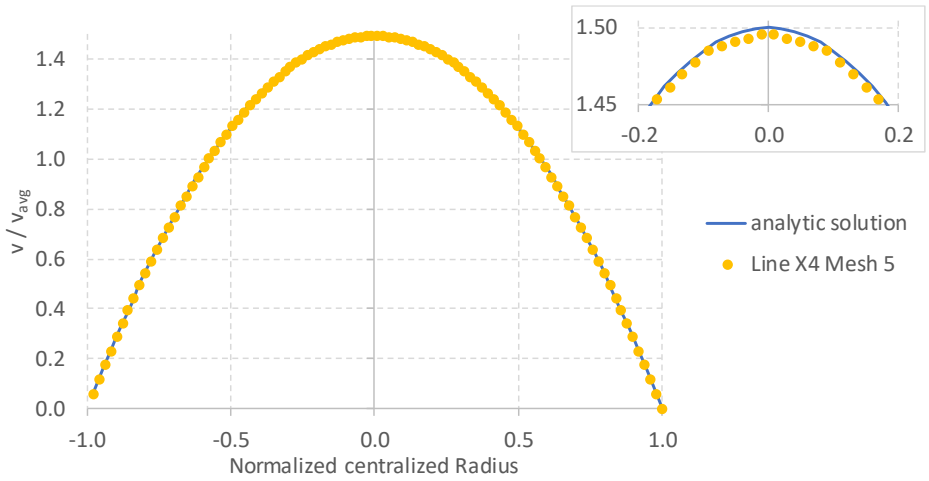

Figure 39 - Comparison between the velocity profile and the analytical solution

The velocity profile obtained replicates almost exactly the analytical profile, with an average error of 2 %.

3.1.3 Thermal Validation

For the thermal validation the same geometry and mesh were considered. Both walls were considered to have a constant temperature. The wall temperature imposed was higher than the inlet oil temperature. The boundary equations used for this analysis can be found in Table 21.

Table 21 - Boundary conditions applied for the thermal verification

Boundary Type	Momentum			Thermal	
	Boundary Condition	U_0 / m s^{-1}	P_0 /Pa	Boundary Condition	T_0 / °C
Inlet	Velocity	0.10	-	Temperature	35
Outlet	Pressure	-	0	-	-
Wall 1	No slip	-	-	Temperature	50
Wall 2	No slip	-	-	Temperature	50

The heat transferred to the fluid can be expressed as

$$\dot{Q} = \dot{m} * \int_{T_{in}}^{T_{out}} C_p \, dT \tag{17}$$

where $\dot{m}$ is the mass flow rate, C_p is the oil specific heat, T_{in} is the average inlet oil temperature and T_{out} is the average outlet oil temperature. *Fluent* can automatically output the value of $\dot{Q}$. It can also be calculated using equation 17, with T_{out} obtained via simulation, an average value of C_p considering the fluid properties with T_{in} and T_{out}. The comparison between both values can be found in Table 22.

Table 22 – Comparison of Heat flux obtained via simulation and equation 17

$\dot{Q}_{Fluent}$ / W	$\dot{Q}_{calculated}$ / W	Deviation
680	676	0.6 %

To have a deeper understanding and verification of the results obtained the calculation of $\dot{Q}$ can also be done by the heat flux that is released by the walls.

The heat flux from the walls to the oil can be defined as [48]

$$\dot{Q} = h * A * (T_{wall} - T_{oil}) \tag{18}$$

where h is the heat transfer coefficient, A is the area through which the heat transferred, T_{wall} is the temperature of the wall and T_{oil} is the reference temperature of oil.

The value of the heat transfer coefficient is calculated with the Nusselt number (Nu). The Nusselt number is given by [48]

$$Nu = \frac{h \, L_c}{k} \tag{19}$$

where L_c is the characteristic length and k is the thermal conductivity. Nu represents the ratio between the convective heat transfer and the conductive heat transfer. The characteristic length depends on the geometry chosen. In this case, L_c is equal to the hydraulic diameter D_h.

The Nusselt number of flow between isothermal parallel plates of length L can also be given by [48]

$$Nu = 7.54 + \frac{0.03\left(\frac{D_h}{L}\right) Re\ Pr}{1 + 0.016[\left(\frac{D_h}{L}\right) Re\ Pr]^{2/3}} \tag{20}$$

where Re is the Reynold number and Pr is the Prandtl number.

The hydraulic diameter can be given by

$$D_h = \frac{4A}{P} \tag{21}$$

where A is area of the cross section and P is the perimeter. For a rectangular geometry

$$D_h = 2H \tag{22}$$

where H is the height of the pass. The hydraulic diameter in this geometry is then equal to 0.006 m. Using equation 20, the Nusselt number obtained was 17.3. The heat transfer coefficient was the calculated using equation 19 and is equal to 380 W m^{-2} $^{\circ}C^{-1}$. Finally, using equation 18, the heat flux obtained for a single wall was 332.15 W, making the total heat flux 664.30 W. The error obtained when compared with the value given by *Fluent* shown in Table 22 is 2.4 %.

Appendix 4 - Other Results

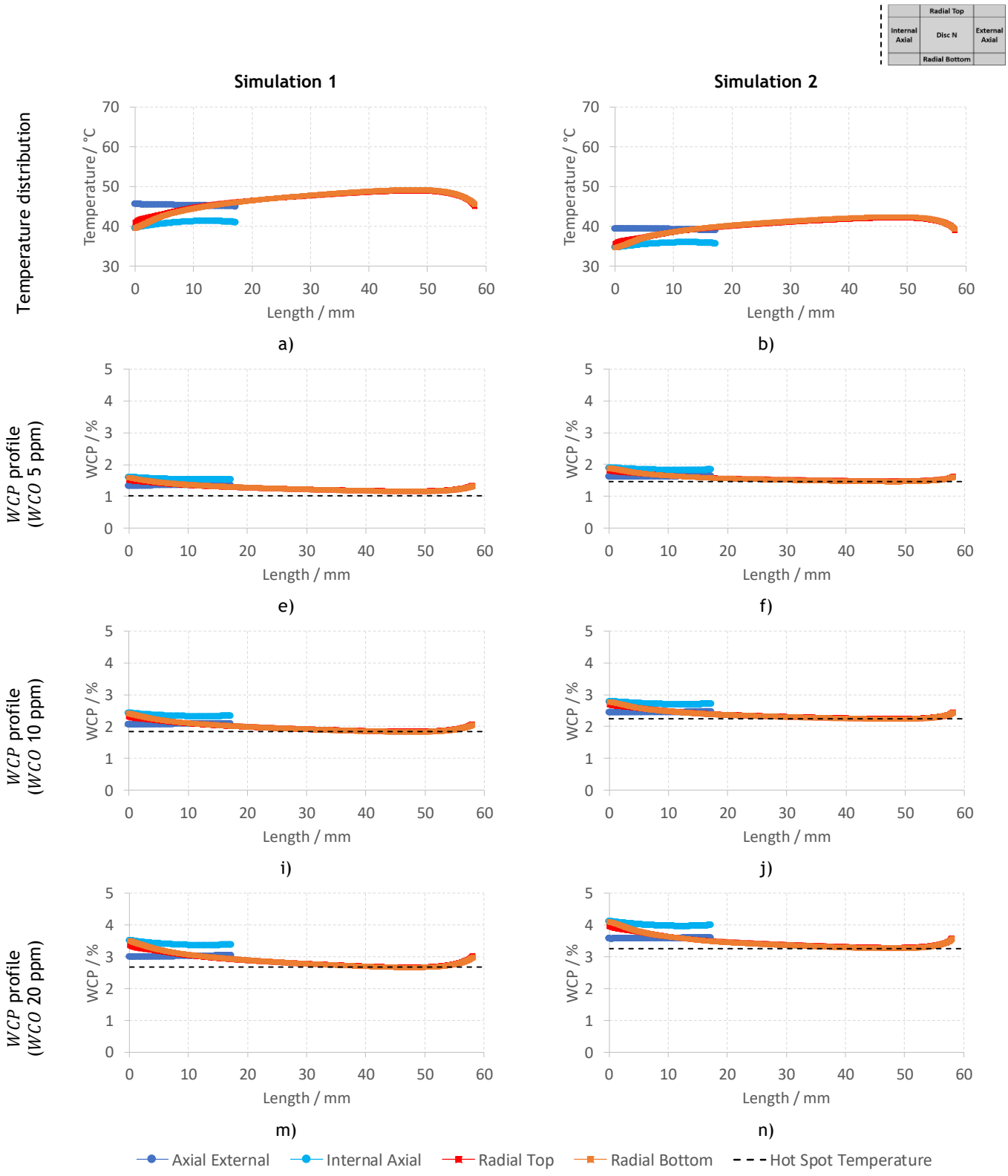

Figure 40 - Temperature (a, b, c, d) and WCP profiles (e to p) obtained for disc 51; The paper water content was calculated assuming different temperatures (each surface of the disc and the hot spot value), for three values of inlet water content in oil (WCO): 5, 10 and 20 ppm

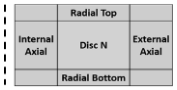
Radial Top
Internal Axial
Disc N
External Axial
Radial Bottom

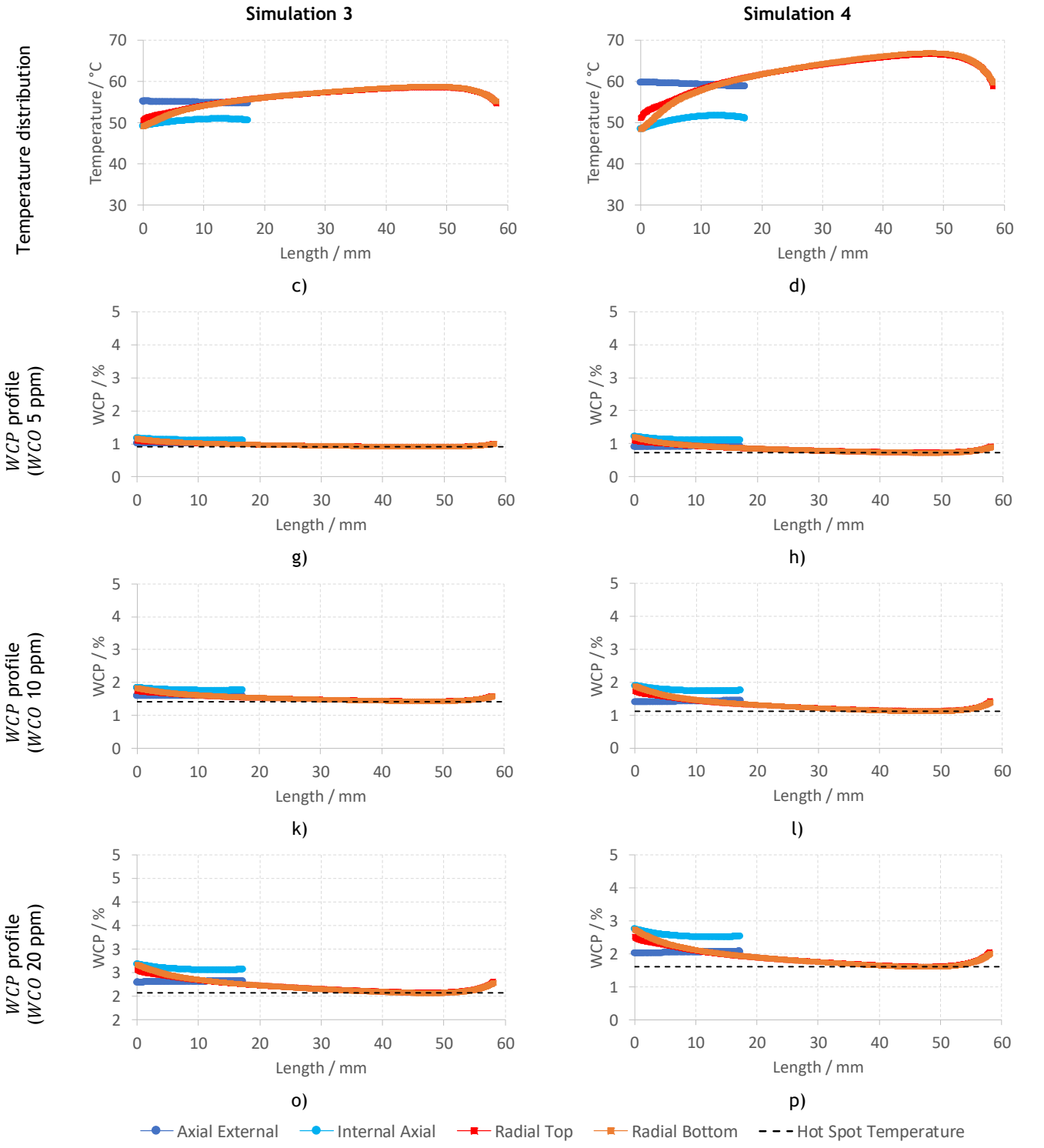
Simulation 3
Simulation 4
Temperature distribution
Temperature / °C
Length / mm
c)
d)
WCP profile (WCO 5 ppm)
WCP / %
g)
h)
WCP profile (WCO 10 ppm)
k)
l)
WCP profile (WCO 20 ppm)
o)
p)
Axial External
Internal Axial
Radial Top
Radial Bottom
Hot Spot Temperature

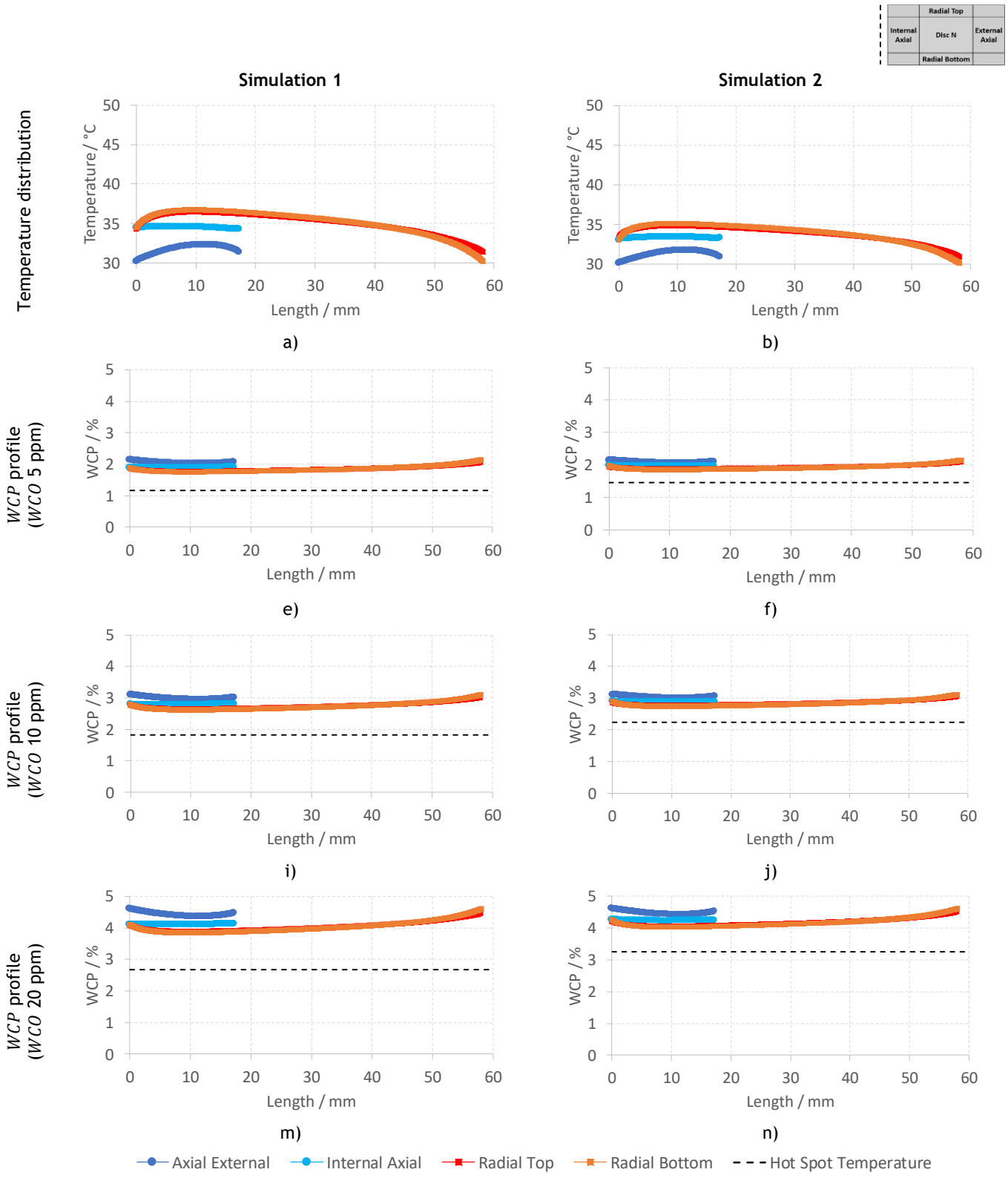

Figure 41 - Temperature (a, b, c, d) and WCP profiles (e to p) obtained for disc 9; The paper water content was calculated assuming different temperatures (each surface of the disc and the hot spot value), for three values of inlet water content in oil (WCO): 5, 10 and 20 ppm

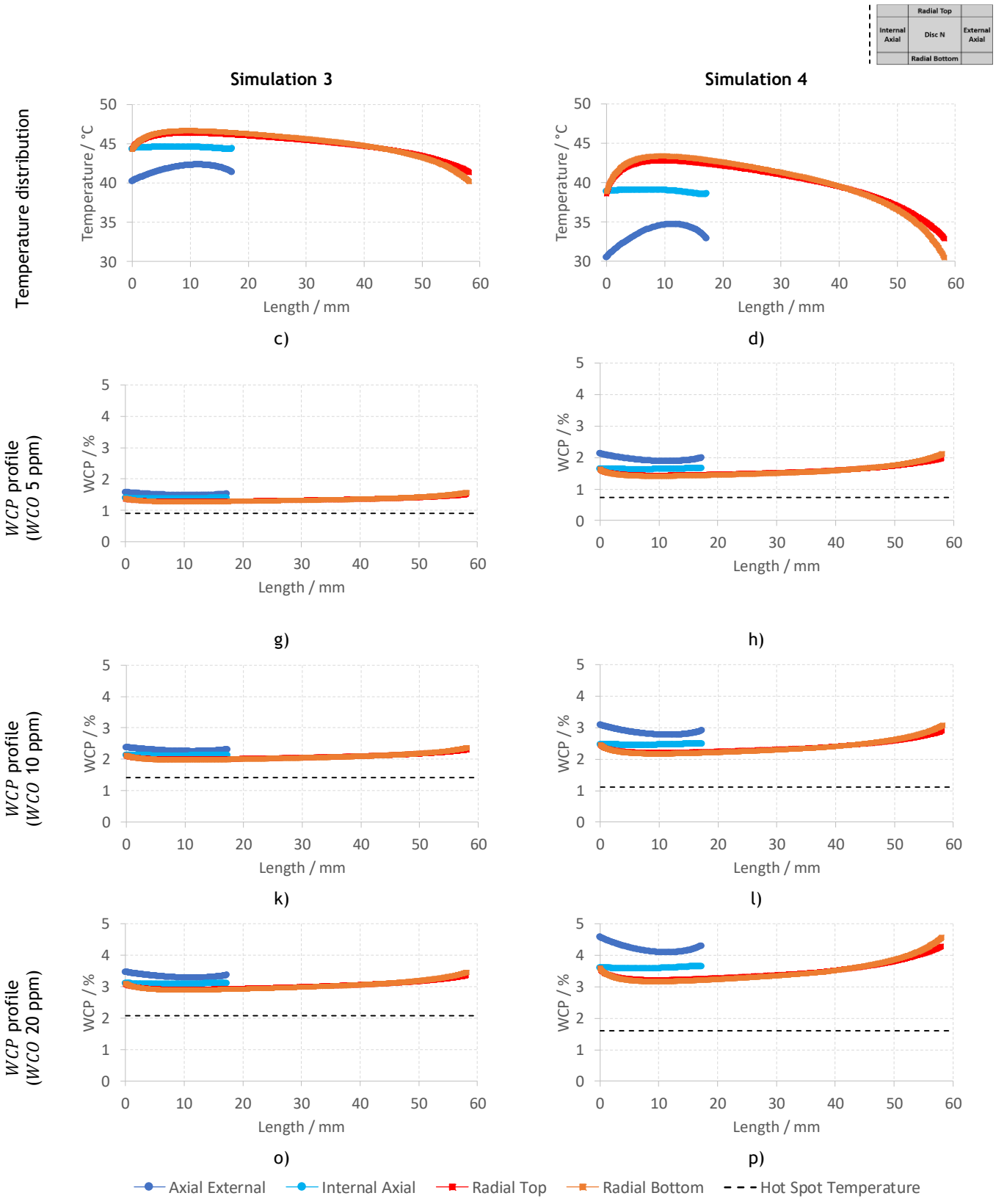
Radial Top
Internal Axial
Disc N
External Axial
Radial Bottom
Simulation 3
Simulation 4
Temperature distribution
Temperature / °C
Length / mm
c)
d)
WCP profile (WCO 5 ppm)
WCP / %
g)
h)
WCP profile (WCO 10 ppm)
k)
l)
WCP profile (WCO 20 ppm)
o)
p)
Axial External
Internal Axial
Radial Top
Radial Bottom
Hot Spot Temperature

Table 23 – Maximum and minimum temperature and WCP wall values and their gradients in disc 51

		Axial External				Axial Internal				Radial Top				Radial Bottom			
		T / °C	WCP 5ppm	WCP 10ppm	WCP 20ppm	T / °C	WCP 5ppm	WCP 10ppm	WCP 20ppm	T / °C	WCP 5ppm	WCP 10ppm	WCP 20ppm	T / °C	WCP 5ppm	WCP 10ppm	WCP 20ppm
Simulation 1	min	44.9	1.32	2.05	2.99	39.5	1.51	2.30	3.36	40.9	1.17	1.84	2.69	39.5	1.16	1.83	2.67
	max	45.5	1.35	2.09	3.04	41.2	1.60	2.41	3.52	49.0	1.53	2.32	3.39	49.1	1.60	2.41	3.52
	Δ	0.6	0.03	0.04	0.05	1.7	0.08	0.11	0.16	8.1	0.36	0.48	0.70	9.6	0.43	0.58	0.85
Simulation 2	min	39.0	1.61	2.43	3.55	34.6	1.81	2.68	3.95	35.6	1.47	2.25	3.28	34.6	1.46	2.23	3.26
	max	39.3	1.63	2.45	3.59	35.9	1.88	2.77	4.09	42.2	1.82	2.70	3.98	42.4	1.88	2.77	4.09
	Δ	0.3	0.02	0.03	0.04	1.3	0.07	0.09	0.15	6.6	0.35	0.45	0.70	7.8	0.42	0.54	0.84
Simulation 3	min	54.6	1.00	1.57	2.29	49.2	1.10	1.75	2.55	50.6	0.92	1.43	2.08	49.2	0.92	1.43	2.07
	max	55.2	1.01	1.60	2.32	50.9	1.16	1.83	2.67	58.7	1.11	1.76	2.56	58.8	1.16	1.83	2.67
	Δ	0.5	0.01	0.02	0.03	1.7	0.06	0.08	0.12	8.1	0.19	0.33	0.48	9.6	0.25	0.40	0.60
Simulation 4	min	58.7	0.89	1.39	2.01	48.3	1.09	1.72	2.50	51.0	0.73	1.13	1.63	48.3	0.72	1.12	1.61
	max	59.7	0.92	1.43	2.08	51.6	1.20	1.88	2.74	66.5	1.10	1.74	2.54	66.9	1.20	1.88	2.74
	Δ	1.0	0.02	0.04	0.06	3.3	0.11	0.16	0.24	15.5	0.37	0.61	0.91	18.5	0.47	0.77	1.14

Table 24 - Maximum and minimum temperature and WCP wall values and their gradients in disc 9

		Axial External				Axial Internal				Radial Top				Radial Bottom			
		T / °C	WCP 5ppm	WCP 10ppm	WCP 20ppm	T / °C	WCP 5ppm	WCP 10ppm	WCP 20ppm	T / °C	WCP 5ppm	WCP 10ppm	WCP 20ppm	T / °C	WCP 5ppm	WCP 10ppm	WCP 20ppm
Simulation 1	min	30.2	2.01	2.94	4.36	34.3	1.88	2.77	4.09	31.4	1.77	2.64	3.88	30.2	1.76	2.62	3.85
	max	32.3	2.14	3.09	4.60	34.6	1.90	2.80	4.13	36.5	2.07	3.01	4.46	36.7	2.14	3.09	4.60
	Δ	2.1	0.12	0.15	0.24	0.3	0.02	0.02	0.04	5.1	0.29	0.37	0.58	6.5	0.38	0.48	0.75
Simulation 2	min	30.1	2.05	2.98	4.43	33.0	1.95	2.86	4.23	30.9	1.87	2.56	3.76	30.1	1.85	2.61	3.83
	max	31.7	2.14	3.10	4.61	33.4	1.97	2.89	4.28	34.8	2.10	3.03	4.50	35.1	2.14	3.10	4.62
	Δ	1.6	0.09	0.12	0.19	0.4	0.02	0.03	0.04	3.9	0.23	0.47	0.74	5.0	0.29	0.50	0.79
Simulation 3	min	40.2	1.47	2.24	3.27	44.3	1.37	2.11	3.07	41.3	1.29	1.82	2.66	40.2	1.27	1.87	2.73
	max	42.3	1.56	2.37	3.45	44.6	1.38	2.12	3.09	46.4	1.51	2.29	3.34	46.7	1.56	2.37	3.46
	Δ	2.1	0.09	0.12	0.18	0.3	0.01	0.02	0.02	5.0	0.22	0.46	0.68	6.4	0.29	0.50	0.73
Simulation 4	min	30.5	1.88	2.77	4.09	38.5	1.62	2.45	3.58	32.8	1.44	1.92	2.79	30.5	1.42	2.02	2.95
	max	34.7	2.12	3.08	4.57	39.1	1.66	2.49	3.64	42.8	1.98	2.90	4.29	43.4	2.12	3.09	4.60
	Δ	4.2	0.24	0.31	0.49	0.6	0.03	0.04	0.07	10.0	0.54	0.98	1.50	12.9	0.70	1.07	1.65